The role of epithelial primary cilium in the development of hydrocephalus

Ph.D. dissertation

Boglárka Banizs, M.D.

Semmelweis University

Doctoral School of Basic Medicine

Mentor: **Bradley K. Yoder, Ph.D.,** Professor, Department of Cell Biology, University of Alabama at Birmingham, Birmingham, AL, USA

Tutor: **László Rosivall, M.D., Ph.D., D.Sc.** Professor, Director of Renal Research and Training Center, Institute of Pathophysiology, Semmelweis University

Program Leader: **László Rosivall, M.D., Ph.D., D.Sc.**

Official Academic Reviewers: **Tamás Ivanics, M.D., Ph.D.**

President of the Examining Committee: **Emil Monos, M.D., Ph.D., D.Sc.**

Examining Committee Members:

István Nyári M.D., Ph.D.

Zoltán Benyó, M.D., Ph.D.

2009, Budapest

TABLE OF CONTENT

LIST OF ABBREVIATIONS

$[Cl^-]$	Chloride ion concentration
$[HCO_3^-]$	Bicarbonate ion concentration
$[K^+]$	Potassium ion concentration
$[Na^+]$	Sodium ion concentration
ADPKD	Autosomal dominant polycystic kidney disease
AE2	Anion Exchanger-2
AQP1	Aquaporin-1 water channel
ARPKD	Autosomal recessive polycystic kidney disease
cAMP	Cyclic adenosine monophosphate
CA II	Carbonic Anhydrase type II
CAXII	Carbonic Anhydrase type XII
CFTR	Cystic fibrosis transmembrane conductance regulator
ClC-2	Chloride-ion channel-2
Cl^-	Chloride ion
CNS	Central nervous system
CP	Choroid plexus
CSF	Cerebrospinal fluid
DIDS	4,4'-diisothiocyanatostilbene-2,2'-disulfonic acid
ENaC	Epithelial sodium channel
H^+	Hydrogen ion/proton
HCO_3^-	Bicarbonate ion
IFT	Intraflagellar transport
KAP	Kinesin superfamily-associated protein
KCC3	Potassium/Chloride cotransporter-3
KCC4	Potassium/Chloride cotransporter-4
KIF3A	Kinesin-like protein 3A
KIF3B	Kinesin-like protein 3B
Kir7.1	Inwardly rectifying K^+ channel
Kv1.1	Delayed-rectifying K^+ channel
Kv1.3	Delayed-rectifying K^+ channel
Na^+	Sodium ion

Na^+/K^+-ATPase	Sodium/ Potassium ATPase pump
NaCl	Sodium Chloride
$NaHCO_3$	Sodium bicarbonate
NBCe2	Electrogenic Sodium-Bicarbonate cotransporter-2
NBCn1	Electroneutral Sodium-Bicarbonate cotransporter-1
NCBe	Electrogenic Sodium-Bicarbonate cotransporter
NHE1	Sodium/ hydrogen ion exchanger-1
NHE3	Sodium/ hydrogen ion exchanger-3
NHE8	Sodium/ hydrogen ion exchanger-8
NKCC1	Sodium/ Potassium/Chloride cotransporter-1
NKCC2	Sodium/ Potassium/Chloride cotransporter-2
pH_i	Intracellular pH
PKA	Protein kinase A
V2R	Vasopressin 2 receptor

INTRODUCTION

Hydrocephalus

Hydrocephalus is a progressive pathological condition characterized by an excessive accumulation of cerebrospinal fluid (CSF) in the brain ventricles. It can be caused by impaired CSF flow, excess CSF production, or lack of CSF reabsorption and is one of the most common anomalies of the central nervous system affecting up to 1 in 1,000 children. Hydrocephalus is classified as either communicative or obstructive depending whether CSF flow is blocked along the ventricular system. Obstructive forms of hydrocephalus are the most common, although it remains a matter of controversy whether many of the obstructive forms arise from communicative forms as a consequence of pathology associated with ventricular expansion (11, 21).

The treatment strategies for hydrocephalus currently in use were established in the middle of the last century and involve surgical insertion of a ventricular shunt to facilitate drainage of excess CSF. However, shunt infections or malfunctions frequently necessitate surgical revision. The failure rate of these shunts can be as high as 40% a year after insertion and 50% at two years and thus this treatment strategy represents a lifetime commitment for the child and family, that involves significant morbidity and mortality. Despite the high prevalence of hydrocephalus in children, in most cases the molecular mechanism(s) leading to the pathology has remained elusive (11, 21). Thus, in order to develop alternative treatment strategies, a better understanding of the causes of this disease is desperately needed.

The mammalian ventricular system

The brain ventricles are a series of interconnected cavities within the central nervous system that contain the cerebrospinal fluid. In adults, the ventricles are lined by "leaky" epithelia called ependymal cells that possess large amounts of motile cilia on their apical surface (Figure 1). The beating of these cilia is thought to facilitate movement of CSF through the ventricles and several models of hydrocephalus have been associated with defects in the motion or formation of these cilia (28).

The ependymal cells lining the ventricles are continuous with the epithelia of the choroid plexus, a leaf-like structure extending into the ventricle lumen. Unlike the

ependyma, the choroid plexus epithelia have extensive tight junctions that prevent free paracellular movement between the blood and CSF (see details below). (18, 60).

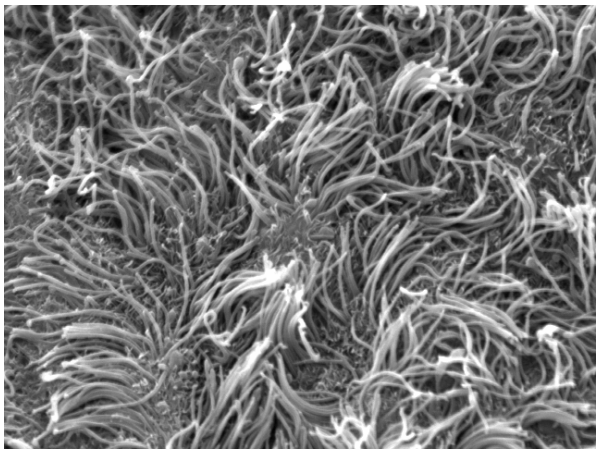

Figure 1. Scanning electronmicroscopic image of the ependyma isolated from the 4th ventricle of a healthy, young adult mouse. The ependymal lining possesses abundant long motile cilia that assure fast CSF flow through the ventricles by synchronized beating. (4000 X magnification)

Structure of the choroid plexus

The mammalian choroid plexus tissue forms characteristic sheet-like structures in the left and right lateral ventricles, and branched, villi-like structures in the 3rd and 4th ventricles of the brain. Both types of structures consist of a single continuous layer of epithelial cells residing on a core of sparse connective tissue, which carries blood vessels of different caliber from small arteries through capillaries to small veins. The surface cells are of similar origin as the ependymal cells lining the remaining ventricular surface(48, 61).

Electron microscopic analyses have revealed that the cuboidal to cylindrical epithelial cells of the choroid plexus display highly differentiated cell surfaces (Figure 2). The ventricular or luminal surface is characterized by numerous microvilli, while the basal surface appears remarkably smooth, whereas the lateral surface is convoluted, with interdigitations between the basal parts of adjacent cells. These structures represent a substantial increase of the surface area like the microvilli, which increase the luminal surface by 10-fold, approximately. Both surface area enlargements are thought to be important for the transport capability of the epithelium (48).

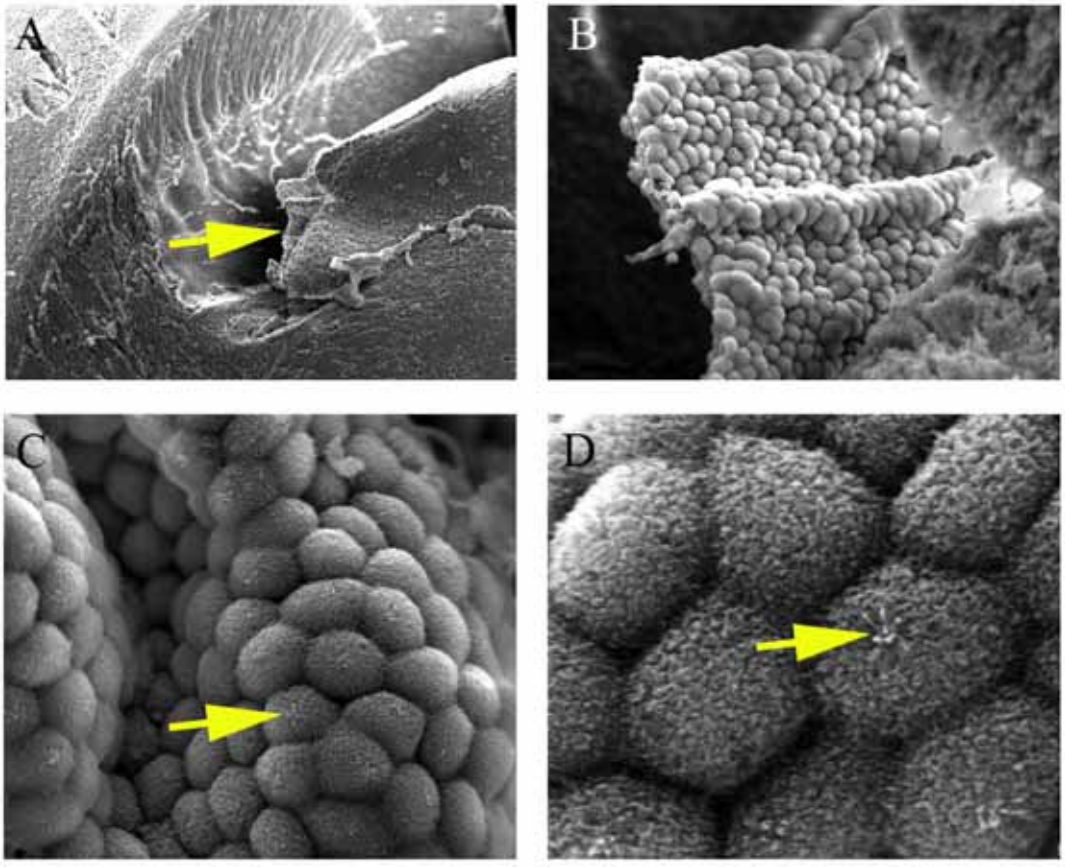

Figure 2. Scanning electronmicrographs of the choroid plexus from a healthy young adult mouse. A: shows cross-section of the lateral ventricle, yellow arrow points to the choroid plexus. (60 X magnification) B: higher magnification of the region seen on panel A with a leaf-like choroid plexus. (450 X magnification) C: closer look of the choroid plexus tissue surface, arrow points to the tuft of cilia. (1500 X magnification) D: choroid plexus cells demonstrate villus-like structures to increase cell surface. Arrow points to the group of cilia. (4000 X magnification)

Production and Functions of the Cerebrospinal Fluid

Cerebrospinal fluid (CSF) has several essential functions in the central nervous system. It provides buoyancy and physical support for the brain, buffering changes in intracranial blood volume or pressure. The CSF acts as a specialized extracellular environment that mediates removal of metabolic by-products and facilitates transport of nutrients and hormones throughout the brain and it is needed for signaling during

development. Thus, regulating the production and composition of CSF is essential for normal neuronal function.

The composition of CSF is very similar to that of plasma with the exception being that CSF has reduced amounts of protein; however, CSF is not simply an ultra-filtrate of the plasma but rather a regulated secretory product generated largely by the choroid plexus epithelia. The CSF is slightly hypertonic compared to plasma and the [Na^+] and [HCO_3^-] are slightly higher than expected at equilibrium, while [K^+] and [Cl^-] are lower in the CSF. Also, there is a modest positive electrical potential difference across the epithelium, i.e. up to 5 mV lumen positive (2, 48, 60).

The ionic composition of nascent CSF consists mainly of NaCl and $NaHCO_3$, and the production rate is strictly coupled to the rate of Na^+ secretion. In contrast to other secreting epithelia, Na^+ is actively pumped across the choroid plexus luminal membrane by the Na^+/K^+ATPase with possible contributions by other Na^+ transporters, e.g. the luminal $Na^+/K^+/2Cl^-$ cotransporter. The Cl^- and HCO_3^- ions are likely transported by a luminal cAMP-activated inward rectified anion conductance. The task of basolateral transport processes is to translocate Na^+, Cl^- and HCO_3^- across the plasma membrane with virtually the same proportion of the major ions as in the nascent CSF. Water molecules are driven by osmotic gradient across the epithelium, mainly through water channels. Thus, as in most other epithelia, fluid secretion in choroid plexus is dependent on the unidirectional transport of ions. This occurs through the polarized distribution of ion transport proteins in either the luminal or basolateral membranes (10, 48). Figure 3 summarizes the mechanism of CSF production and localization of the most important transporters at the current level of understanding.

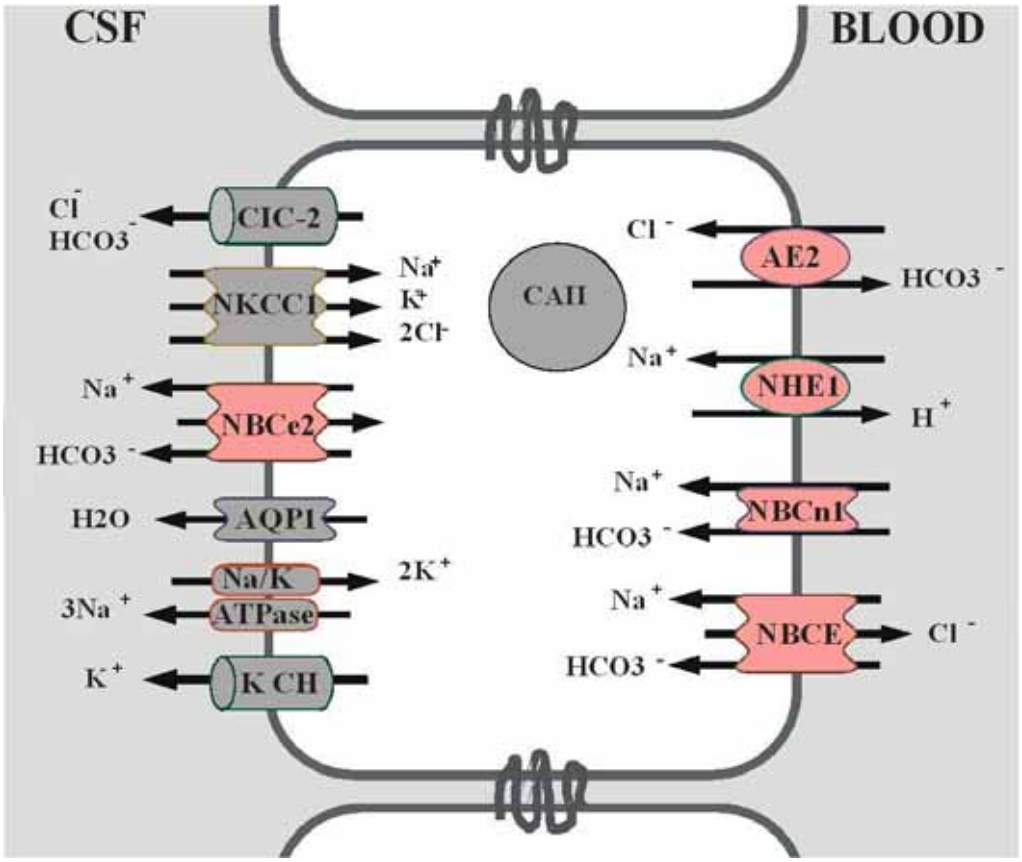

Figure 3. Schematic representation of the ion and water transporters/channels in the choroid plexus epithelium. Na^+/K^+-ATPase and the $Na^+/K^+/2Cl^-$ cotransporter (NKCC1) are strictly luminal plasma membrane transport proteins. K CH represents all apical K^+ channels. ClC-2 corresponds to the anion conductance of the cAMP-sensitive ClC-2 like channel. The electrogenic NBCe2, a Na^+/HCO_3^- cotransporter is also found at the luminal membrane. AQP1, aquaporin1 water-channel, is expressed mostly on the luminal membrane, and the carbonic anhydrase, CA II is found in the cytosolic compartment. Three HCO_3^- transporters are localized to the basolateral membrane along with a Na^+/H^+ exchanger: the base extruder AE2 and the two Na^+-base loaders, NBCn1 and NCBe. *Note: only the most important transport proteins are shown on the figure.

A. Apical transport events

Na^+/K^+ATPase. This ouabain-sensitive transporter located on the luminal plasma membrane is considered to be responsible for the majority of transepithelial Na^+ flux. The Na^+/K^+-ATPase mediates the secretion of 3 Na^+ into the CSF and reabsorption of 2 K^+ from the CSF against their concentration gradients (48).

$Na^+/K^+/2Cl^-$ cotransporter. The furosemide-sensitive $Na^+/K^+/2Cl^-$ cotransporter may also contribute to Na^+ secretion to the CSF. The molecular identity of this luminal transport in the choroid plexus was shown to be NKCC1. In other epithelia this transporter is localized to the basolateral surface and only the related protein, NKCC2, of the renal thick ascending limbs is expressed luminally. In any case, Na^+ and K^+ are cotransported with 2 Cl^- ions into cells, as the collective inward Na^+ and Cl^- gradients by far exceed the outward K^+ gradient, given typical ionic gradients. However, the NKCC1 in the choroid plexus has been reported to transport in both an inward and outward directions. A remarkably high intracellular [Na^+] (and [Cl^-]) and a relatively low [K^+] concentration in CSF actually point towards a net outward transport by NKCC1 in the choroid plexus. In addition to NKCC1, a furosemide-sensitive apical K^+ and Cl^--dependent KCC4 has been proposed in CSF secretion by recycling K^+ to the lumen, thereby supporting ongoing Na^+/K^+-ATPase activity, simultaneously with mediating Cl^- secretion (45, 48).

Cl^- and HCO_3^- channels. DIDS is a relatively unspecific blocker of many Cl^- channels and Cl^-/HCO_3^- transporters. As in other epithelia, Cl^- and HCO_3^- seem to be secreted mainly by luminal electrogenic processes. Two major anion conductances, both inward rectifiers, have been found on the choroid plexus epithelia. One is a volume-sensitive anion conductance, while the other is a protein kinase A (PKA)-activated anion conductance with a high permeability to both Cl^- and HCO_3^-. Based on previous publications neither CFTR nor ClC-2 channels are expressed on mammalian CP epithelia, though a cAMP-regulated ClC-2-like anion channel (based on published patch-clamp studies) is thought to be responsible for the majority of luminal secretion of Cl^- and HCO_3^- (10, 48).

K^+ channels. The luminal K^+ conductance in mammalian choroid plexus is driven by Kir7.1, an inwardly rectifying K^+ channel and two delayed-rectifying K^+ channels,

Kv1.1 and Kv1.3, all confined to the apical surface. The K^+ channels are thought to set the membrane potential of the epithelial cells and to sustain the Na^+/K^+-ATPase by providing an efflux pathway for K^+ (in addition to NKCC1 and KCC4) (10, 48).

B. Basolateral transport events

Na^+/H^+ exchange. Amiloride-sensitive NHE1 has been suggested to work on the basolateral surface of the CP epithelia. In the current model of CSF formation, the NHE would be capable of ridding the cell of protons formed by the hydration of CO_2 and subsequent dissociation of carbonic acid to HCO_3^- and H^+, and in the same process provide the Na^+ necessary to sustain CSF secretion. Surprisingly, amiloride has little effect on Na^+-dependent pH recovery in the choroid plexus in the presence of CO_2/HCO_3^- in vitro. This suggests that the Na^+/H^+exchanger plays a minor role in maintaining the pH_i under these conditions. The exact role of NHE1 along with the recently discovered NHE3 and NHE8 in CP epithelia remains to be clarified.

Na^+ channels. The molecular and functional expression of the epithelial Na^+ channel, ENaC, was reported for the choroid plexus. The authors found the ENaC at the basolateral surface and suggested it to participate in Na^+ loading mechanism. However, further analysis of this channel is required (48).

HCO_3^- transporters. The basolateral electroneutral $Cl^-/HCO3^-$ exchanger AE2 is a DIDS-sensitive base extruder to maintain pH_i in many cells, e.g. the distal renal tubules and collecting ducts. AE2 has been involved in HCO_3^- reabsorption, which may in fact be its net effect in the choroid plexus. Thus, the protein is not likely to participate in the HCO_3^- secretion, but may well support luminal Cl^- secretion by loading this ion into the cells from the basolateral side. Other functions of AE2 may include cell-volume regulation working in concert with e.g. the NHE1 or simply protection of the cells against alkalinization (48).

Two $NaHCO_3$ transporters were demonstrated in the basolateral plasma membrane of CP epithelial cells, which could also represent basolateral Na^+ uptake pathways. NCBe is an electroneutral DIDS-sensitive $NaHCO_3$ importer that likely also extrudes Cl^- with a proposed stoichiometry equivalent to the uptake of 1 Na^+, and $2HCO_3^-$ for the extrusion of $1Cl^-$. NCBe was currently suggested as a major Na^+-entry route into the

cell. It is also proposed to be one of the major contributors for setting pH_i. In contrast, the second electroneutral basolateral $NaHCO_3$ transporter, NBCn1 is not likely to play a major role in the transepithelial movement of Na^+, but might serve to correct intracellular acidosis in the CP epithelia (48).

K^+/Cl^- cotransport. KCC3 has been identified in the CP epithelia. This mechanism, to date, represents the only known K^+ efflux pathway from cells to blood.

Carbonic anhydrases. Intracellular CAII and extracellular membrane bound CAXII are functionally and physically coupled to transporters of the SLC4a family (as AE2, and electrogenic NBC). They catalyze the conversion of CO_2 and H_2O into HCO_3^- and H^+ that are subsequently exchanged for Na^+ and Cl^- across the basolateral membrane, the net effect being accumulation of intracellular Na^+ and Cl^-.

Water channels. Water transport across the epithelium is driven by the modest luminal hyperosmolarity. The small osmotic gradient and the high rate of water transport resemble that of the renal proximal tubules. The water channel AQP1 was found to be abundantly expressed apically and at moderate levels on the basolateral side (48).

Regulation of CSF production. Regulatory factors of CSF production are hemodynamics, metabolism of nutrients and hormones. Among the most interesting discoveries are the detection of vasopressin-1 receptors and receptors for atrial natriuretic factor, angiotensin II, endothelin-1, serotonin, bradykinin and insulin. It is noteworthy that although many of the mediators are found in blood; the transport pathways of the choroid plexus seem relatively resistant to changes in these plasma levels (48). From the point of view of our work vasopressin-1 receptors have special interest which will be discussed later (see below).

CSF Circulation

Most of the CSF is produced by the choroid plexi located in the lateral ventricles. From the lateral ventricles CSF flows through the foramina of Monro into the third ventricle, through the aqueduct of Sylvius into the fourth ventricle and through the foramina Lushka and Magendie to the cisterna magna where it moves dorsally into the subarachnoid spaces and is reabsorbed by the Pacchioni granulations. An imbalance in the rate of production and reabsorption or a disruption in the movement of the CSF, as occurs in aqueduct stenosis, results in pathologies such as hydrocephalus. While many

investigators have considered duct stenosis as the initiating event in the disease, others have regarded duct obstruction as a secondary consequence of compression exerted by the expanding ventricles.

Although the mechanisms driving CSF movement are largely unknown several factors are thought to be involved. This includes the hydrostatic gradient resulting from continued production of CSF, pulsation of the arterial tree, and the wave-like beating of cilia on the ependymal cells. The importance of the cilia has been supported by the hydrocephalus that develops in patients with primary cilia dyskinesia as well as in the *Mdnah5* mutant mice in which cilia beat is impaired (28).

Models for hydrocephalus

Much of our understanding of hydrocephalus has come from the analysis of animal models. H-Tx rats develop congenital hydrocephalus with varying degree of severity. The mechanism leading to the pathology in these animals remains controversial with some studies indicating the primary defect is caused by duct obstruction late in gestation while other studies indicate the hydrocephalus develops prior to impaired CSF flow (30, 34). Mice lacking the *E2F-5* transcription factor cause a form of communicating congenital hydrocephalus. In these mice, the pathology has been attributed to increased secretory activity of the choroid plexus; however, the role of *E2F-5* in CSF production remains unknown (36). The hydrocephalus that develops in the L1 neural adhesion molecule deficient mice, which is mutated in human forms of X-linked hydrocephalus, is initially associated with a patent aqueduct; however, duct stenosis is evident in the mice with severe pathology (52). There are also several mouse models of hydrocephalus that have been attributed to ciliary dysfunction. Disruption of the outer dynein arm protein *Mdnah5* results in impaired cilia motility on ependymal cells. The loss of CSF flow is thought to contribute to the closure of the aqueduct during early postnatal development and the development of hydrocephalus (28, 52). An analogous mechanism may be involved in the pathology of Wic-Hyd rats that also have impaired cilia motility; however, the genetic defect in these mutants has not yet been determined (69). In addition, mice lacking the cilia proteins Spag-6 or hydin, or the transcription factor *Hfh-4* that lack ependymal cell cilia, all exhibit severe forms of hydrocephalus (14, 16, 57). Finally, cilia function in the CSF ventricular system is also important in humans as

evidenced by the incidence of hydrocephalus in human patients with primary ciliary dyskinesia (12). However, it should be noted the possible role of choroid plexus epithelial cilia dysfunction has not been evaluated in any of these models or in human patients.

Mechanism of cilia formation and maintenance

The analysis of flagella from *Chlamydomonas* or cilia from the lung has revealed that this organelle is an extremely complex structure. More than 500 peptides are involved in its formation, maintenance, and functions. Furthermore, since cilia are devoid of ribosomes, the cell must transport the required proteins for assembly and sensory or signaling activity from their site of synthesis in the cytoplasm into the cilia where it is released and integrated into the axoneme. This occurs through a process referred to as intraflagellar transport (IFT) that was first described in *Chlamydomonas* and subsequently found to be conserved in all ciliated eukaryotes. According to this model, proteins involved in flagella formation concentrate near basal bodies, an apparent holding zone for IFT polypeptides, where they preassemble into large particles (IFT particle), and move up the forming flagella through the action of the heterotrimeric kinesin (kinesin-II complex – KIF3A, KIF3B, and KAP). A dynein motor protein then mediates retrograde transport back to the basal body region. One of the proposed roles of the IFT particle is to transport cargo, such as receptors and channels as well as structural proteins, into the axoneme (Figure 4) (58).

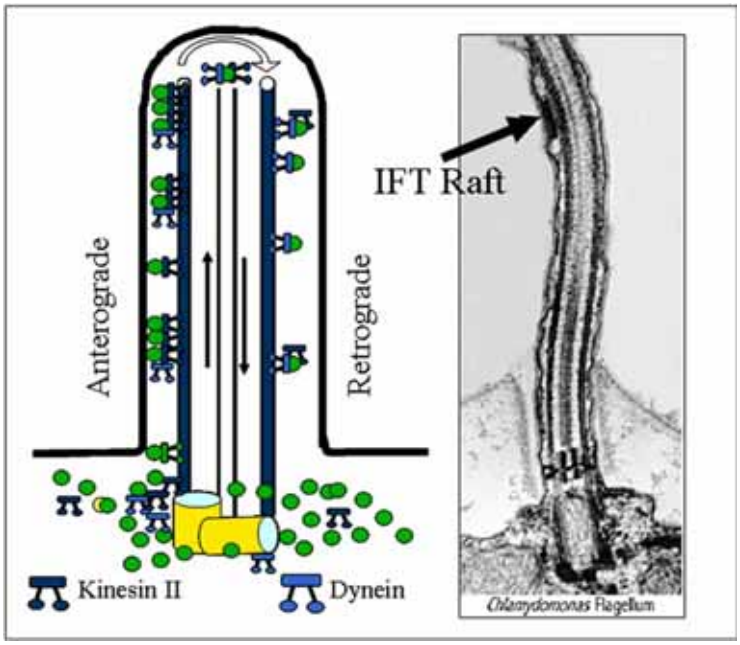

Figure 4. Schematic structure and intraflagellar trafficking of a motile cilium. IFT rafts are assembled at the base of the cilium. Anterograde transport is mediated by kinesin II while retrograde transport is conducted by dynein. Inset shows electromicrograph of a cilium. Arrow points to an IFT raft.

Cilia dysfunction in disease and developmental abnormalities

Cilia and flagella are common organelles present on the surface of nearly every cell in most mammalian tissues. These microtubule-based projections play critical roles in processes ranging from fluid movement, cell motility and cell cycle regulation, to sensory perception that allows a cell or organism to interact efficiently with its environment. For example, epithelia in the lungs and ependymal cells lining the brain ventricles use ciliary projections for movement of mucus and cerebral spinal fluid, respectively. In addition to the motile cilia, there are numerous examples of immotile or primary cilia. One of the main functions of immotile cilia appears to be sensory perception. Primary cilia are present on olfactory neurons where they serve in chemoreception, on the rods and cones of the eyes for photoreception, and on renal epithelia where they act as mechano-transducers that respond to fluid flow through the tubules (47).

Disruption of cilia function in a number of tissues has been associated with the development of severe disease pathologies. In the pancreas, disruption of primary cilia on the islets and ducts results in defects in glucose responses, dilations of the ducts and acinar cell atrophy (13, 78). Loss of primary cilia in the kidney leads to cystic lesion in

tubules with altered calcium and sodium transport (37). Cilia dysfunction in the eye causes retinitis pigmentosa (39). In addition, as indicated in this dissertation, disruption of the cilia on the ependymal or choroid plexus cells in the brain results in hydrocephalus that we believe is due to both impaired CSF flow through the ventricles and to excess CSF production by the choroid plexus.

Motile and immotile cilia also play important roles in developmental patterning. Mice lacking the cilia proteins Kif3A, Kif3B, polaris, or the left-right dynein exhibit random specification of the left-right body axis (63, 65). In all of these mutants, the developmental abnormalities have been attributed to the loss or dysfunction of cilia on the ventral surface of the node, a gastrulation-stage organizing center. These studies reveal that nodal cilia, despite being a single cilium per cell, generate as well as sense a leftward-directed flow across the node surface that is needed to specify the left and right sides of the embryo. Finally, additional data from our group as well as others have uncovered an unexpected role for primary cilia in the sonic hedgehog signaling pathway. Data from our lab indicate that the Gli transcription factors that mediate the hedgehog signaling response localize to the tip of the cilia along with other proteins in the pathway and that in the absence of the cilium these factors are inefficiently processed to their activated or repressor forms.

Tg737 and cilia assembly

Tg737 (now *IFT88*) encodes polaris, a highly conserved protein that was identified through a hypomorphic mutation in the *Oak Ridge Polycystic Kidneys (Tg737^{orpk})* mouse. A role for *Tg737* in ciliogenesis was substantiated by the ciliary defects observed in the *Tg737^{orpk}* mutant mice. In *Tg737^{orpk}* mice the cilia are aberrantly formed on different types of cells (40, 66).

Expression and localization studies along with the phenotypes seen in *Tg737* mutation suggest that *Tg737* function is required for cilia assembly. This was further supported by studies of the *Tg737* homologs in *C. elegans* (*osm*-5), *Drosophila* (*nompB*), *Danio rerio* (*ovl*), and *Chlamydomonas* (*IFT88*) (9, 26, 43, 75, 76). Functional data obtained from studies in these lower eukaryotes reveal that polaris is a highly conserved component of the intraflagellar transport (IFT) particle (54).

Mammalian Tg737 gene and pathology associated with the mutation in Tg737^{orpk} mice

The Oak Ridge Polycystic Kidney (*Tg737^{orpk}*) mouse was described over a decade ago as a model for human recessive polycystic kidney disease. The *Tg737^{orpk}* mouse arose through integration of a transgene into an intron of the *Ift88* gene resulting in a hypomorphic allele (Ift88Tg737Rpw). The Ift88Tg737Rpw mutation through impaired intraflagellar transport (IFT) results in a large variety of pathology (40).

The gross phenotype of the *Tg737^{orpk}* mouse was originally described with a triad of scruffy fur, severe growth retardation, and preaxial polydactyly on all limbs (Figure 5). The *Tg737^{orpk}* mouse is best known for its cystic renal phenotype, which resembles that of human autosomal recessive polycystic kidney disease. It was also the first mammalian model to establish a connection between cystic kidney disease and ciliary dysfunction (35). However, in addition to the cystic kidneys, histological analyses of the *Tg737^{orpk}* mice revealed biliary duct hyperplasia in the liver, acinar atrophy and ductal hyperplasia in the pancreas, hydrocephalus, hair and skin abnormalities, and skeletal patterning defects that include formation of extra digits on the limb buds, supernumerary teeth, and cleft palate (Figure 6) (13, 35, 66, 78, 79).

Figure 5. *Tg737^{orpk}* mutant mouse (in the front) and its wild type littermate (in the back). The mutant mouse is severely growth retarded, shows scruffy fur, a steeper and larger forehead compared to body size suggestive of the presence of hydrocephalus.

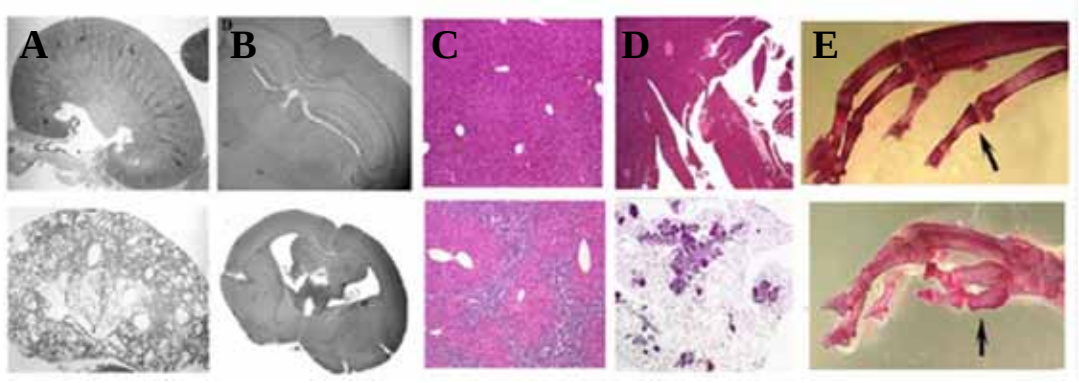

Figure 6. Summary of phenotypes characterized in the Oak Ridge Polycystic Kidney (*Tg737*^{orpk}) mouse. The *Tg737*^{orpk} (FVB/N) mouse (lower panel) has phenotypes in numerous tissues compared with wild-type controls (upper panel). **A.** Cystic lesions are seen in the kidney. **B:** Mutants develop hydrocephalus. **C.** The liver is characterized by bile duct hyperplasia. **D:** In the pancreas, ducts become dilated and acini atrophied **E:** Mutants also exhibit numerous skeletal defects including preaxial polydactyly (arrows).

OBJECTIVES

Our central hypothesis is that cilia function is required for normal regulation of pathways governing CSF production and homeostasis. While cilia on the ependymal cells are motile and loss of motility has been associated with hydrocephalus, the function of cilia on the choroid plexus remains enigmatic. Our primary focus in the present work is to explore connection between cilia dysfunction and the development of hydrocephalus in the *Tg737*^{orpk} mutant mice.

Objectives:

Objective 1 To characterize the development of hydrocephalus in *Tg737* mutant mice by analyzing the initiation and progression of the pathology using MRI imaging techniques and by assessing the effect of *Tg737*^{orpk} mutation on CSF flow.

Objective 2 To determine the effect of cilial dysfunction on epithelial cells of the choroid plexus with determining the composition of the CSF in cilia mutants and

comparing the expression and localization of transport proteins involved in ion transport, water movement, and CSF production in mutant and wild type mice.

Objective 3 To determine if choroid plexus cilia dysfunction results in altered ion transport and excess CSF production by analysis of ion transport properties in mutant choroid plexus.

METHODS AND MATERIALS

Reagents

The dye 2',7'-bis (2-carboxyethyl)-5-(and-6) -carboxyfluorescein, acetoxymethyl ester (BCECF/AM), 4,4'-diisothiocyanatostilbene-2,2'-disulfonic acid, disodium salt (DIDS) and nigericin were purchased from Molecular Probes, Inc. (Carlsbad, CA). Dibutyryl-cAMP and H-89 were purchased from Calbiochem (San Diego, CA). All other reagents were obtained from Sigma (Saint Louis, MO).

Mice

Tg737^{orpk} mice were generated as described previously (40). The lines were maintained as heterozygous crosses on the FVB/N genetic background. Animals were treated and maintained in accordance with the IACUC regulations at the University of Alabama at Birmingham. Genotyping was performed as described previously (76).

Morphological and histological analysis

Brains were fixed within the skull by opening the skull in the parietal region to allow formalin penetration into the tissue. 24-hour postfixation brains were removed and photographed. Fixed brains were then embedded into paraffin blocks and sectioned in coronal plane. Sections were stained with hematoxylin and eosin and photographed.

Magnetic resonance imaging (MRI)

Tg737^{orpk} mutant and wild-type littermates at postnatal day 1 and 6 were anesthetized using 1% isoflurane. MRI was performed on a Bruker-Biospin 8.5T vertical wide-bore DRX-360 (UAB 8.5T Small Animal NMR Facility) with an AVANCE console, a Paravision 3.0.1 software platform, and a Mini0.5 imaging system

equipped with a 56 mm inner diameter gradient set (Billirica, MA). Mice were positioned in a 20-mm birdcage resonator. Images were coronal T2 weighted RARE (8 echoes, rare factor 8) with the following parameters: TR 4.5 sec, effective TE 60ms, FOV 2.5 cm, 256 x 256 matrix, slice thickness 0.45 mm, in plane resolution 98 μm, 4 averages. The body temperature was maintained at 37°C. T2 RARE imaging allows detection of the fluid compartments without requiring the use of contrasting agents. Relative ventricular volume was calculated based on the intensity difference using ImageJ software (NIH, Bethesda).

Immunofluorescence microscopy

Mouse brains were isolated from wild-type and *Tg737*^{orpk} animals and processed for immunofluorescence microscopy as described previously (66). Primary antibody dilutions were used as follows: mouse anti-acetylated α-tubulin 1:1,500, rabbit anti-α-catenin 1:500 (Sigma, St Louis, MI, USA), rabbit anti-polaris antibody 1:500 (BY1700, Sigma-Genosys against amino acids LEIDEDDKYISPSDDPHTN), rabbit anti-polycystin-1 antibody 1:300 (29) and rat anti-zonula occludens 1:40 (from Dr. Daniel Balkovetz, UAB). Secondary antibodies conjugated to FITC and rhodamine Red-X were used at 1:500 (Jackson ImmunoResearch, West Grove, PA). Sections were analyzed by immunofluorescence using an inverted Nikon TE200 microscope and images were captured on a CoolSnap HQ/FX (Roper Scientific, Inc.) CCD camera.

Proliferation analysis

Proliferation in CP cells from day 3 animals was determined by immunostaining with anti-phospho-histone H3 antibody (diluted 1:300, from Upstate, Lake Placid, NY). The proliferation index was assessed by counting H3-positive cell nuclei per 1000 nuclei.

Scanning electron microscopy

Freshly isolated brains from wild-type and *Tg737*^{orpk} mutant animals were processed for scanning electron microscopy as described previously (77). Samples were then analyzed on either ISI SX-40 or Hitachi 2460 Variable Pressure scanning electron microscopes.

Videorecording of ependymal cilia.

Function of ependymal cilia was assessed as described previously (28). Briefly, to capture beating of the ependymal cilia, fresh brain slices from either the lateral or fourth ventricle of day 12 animals were placed on a glass coverslip. Prewarmed phenol red free DMEM/F12 medium was mixed with a suspension of red fluorescent beads (50 μm, Sigma) and added to fresh brain slices. Cilia or particle movement was monitored by differential interference contrast (DIC) and fluorescence microscopy on a Nikon TE200 equipped with a CoolSnap HQ/FX CCD camera. Images were captured at 28 frames/sec using MetaMorph software. The same program was used to track particle movement and to calculate mean speed of the tracked red fluorescent beads.

Brain ventricular injection of fluorescent DiI.

Day 2 and 6 animals were anesthetized using 100 mg/kg ketamine and 5 mg/kg xylazine intraperitoneally. The right lateral ventricle was injected with 1.0 μl of 0.2% DiI using the following coordinates: depth 1.8 mm, lat. 0.9 mm crossing the line which bundle the posterior angles of orbitae bilaterally in 2-day-old mice, 0.8 mm posterior to this point in 6-day-old mice. Mice were then sacrificed and the brains were snap frozen and cryosectioned. Horizontal sections of injected brains were then fixed with 4% paraformaldehyde and nuclei stained with Hoechst. Sections were imaged using fluorescence microscopy. The time required for the dye to pass from the lateral ventricle into the fourth ventricle was determined by analyzing brain sections generated from mice 30, 20, 10 and 5 minutes postinjection.

Isolation of CSF.

To isolate the CSF, 18-23 day wild-type or mutant animals were anesthetized as described above. CSF was harvested using a micromanipulator and Hamilton syringe with a 26-gauge needle with the following coordinates in mutant: Bregma -0.6 mm, lat. 1 mm, depth 1.8 mm and from wild type mice as described previously by DeMattos et al (17). Chloride ion concentration was determined with ion selective microelectrodes following manufacturer's instructions (Lazarlabs, CA).

Determination of $[cAMP]_i$ from isolated choroid plexus.

Choroid plexi isolated from mutant and wild-type brains were immediately frozen in liquid nitrogen. Tissue processing and intracellular cyclic AMP content was determined using a competitive EIA assay system (Zymed Laboratories, CA), following the manufacturer's instructions. Protein content was determined using DC Protein Assay kit (BioRad Laboratories).

Tissue preparation and measurement of pH_i

Day 5 and 6 wild-type and *Tg737^{orpk}* littermates were sacrificed, choroid plexi were removed from the lateral ventricles and placed into a cooled dissection chamber filled with saline solution. Two tissue pieces, freshly isolated from similar regions of choroid plexi obtained from a mutant and wild-type animal were transferred to a thermo-regulated microscope chamber. The preparations were immobilized with glass micropipettes in a position where the epithelium of the two tissue pieces were facing each other (Figure 17). This allowed simultaneous imaging of the two preparations. The tissues were then loaded with BCECF by incubating them in a saline solution containing 10 μmol/L BCECF/AM for 20 minutes. Residual non-hydrolyzed dye was removed before the experiment by flowing saline solution at 2 ml/min for 5 min. During the experiment the bathing solution was exchanged at a rate of 2.5 ml/min. pH_i was measured using a Nikon S Fluor 40x objective and assessed with dual-excitation wavelength fluorescence system, which included a computer-controlled chopper assembly (530 nm emission during alternating 440 and 495 nm light excitation; Photon Technology International, London, Ontario, Canada) and a cooled SenSys charge-coupled camera (Photometrics, Tucson, AZ). Every experiment was calibrated using two pH points with the high-potassium/nigericin technique as described (68). For each experiment the 495/440 nm ratios were converted to pH_i. All experiments were performed at 37 ºC.

Buffering capacity and HCO_3^- flux

To evaluate acid-base transporter activities, we determined the intrinsic buffering power in both wild-type and *Tg737^{orpk}* choroid plexus tissues using the weak acid NH_4^+ (5, 7). These experiments were performed in the nominal absence of CO_2/HCO_3^- and in the absence of external Na^+ to minimize the activity of pH_i regulatory mechanisms. pH_i was

measured in response to stepwise changes in bath NH_4Cl concentration from 20, 10, 1 to 0 mM, and the intrinsic buffering power was calculated at the mean pH_i between steps using the following equation:

$$\beta_i = \Delta[NH_4^+]_i / \Delta pH_i$$

where β_i is the intrinsic buffering capacity, $\Delta[NH_4^+]_i$ is the difference in intracellular ammonium concentration (calculated using pK_a of 8.9 for NH_4^+) and ΔpH_i is the measured change in pH_i.

As shown in Figure 7, the intrinsic buffering capacity displayed a linear decrease with higher pH_i values. The intrinsic buffering power values at varying pH_i were not significantly different in the wild-type and mutant CP epithelia. We therefore pooled the data from both tissues and the intrinsic buffering power (in mmol/L) as a function of pH_i was best fit with the equation:

$$\beta_i = -107.54 \times pH_i + 768.03$$

The initial net acid extrusion (J_{net}) was calculated using the following formula:

$$J_{net} = dpH_i/dt \times (\beta_i + \beta_{CO2})$$

where dpH_i/dt is the initial rate of change in pH_i (over 30 seconds) and β_{CO2} is the buffering capacity conferred by bicarbonate, computed from the theoretical relationship:

$$\beta_{CO2} = 2.3 \times [HCO_3^-]_i$$

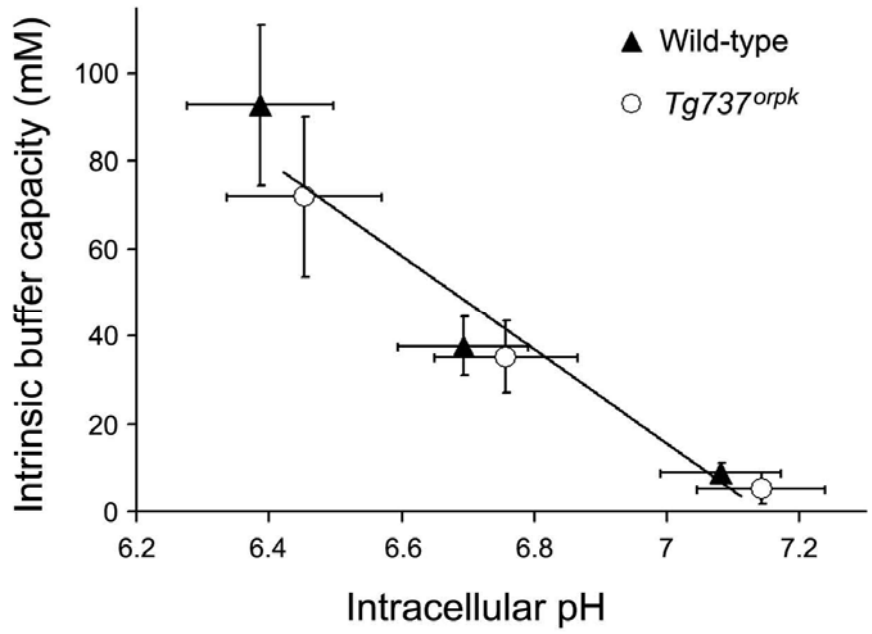

Figure 7. Graph showing the intrinsic buffering capacity of the choroid plexus epithelia from wild-type and *Tg737*^{orpk} mice as a function of pH_i. Data points represent the average values from 3 pairs of preparations. Line represents linear fit to the pooled data from wild-type and mutant tissues.

Statistical analysis

Values are means ± SE. Statistical significance was determined using unpaired Student's t-test in the following experiments (the listed experiments below assess differences between wild type and mutant animals): relative ventricular volume intensity differences; proliferation analysis; particle movements over ependymal cilia; differences in $[cAMP]_i$ and $[Cl^-]$.

Paired Student's *t*-test was used for data analysis in the physiologic experiments, where the wild type and mutant tissues were simultaneously assayed, and where $P < 0.05$ was considered significant. The data from the intrinsic buffering capacity experiments were analyzed by two-way repeated-measures ANOVA.

Solutions

Table 1. below provides the composition of each solution used in our experiments. The pH of the solutions was adjusted to 7.4 at 37 °C. The osmolarity of all solutions was determined with a freezing point depression osmometer and was adjusted with mannitol.

Table 1. Solutions used in the experiment

Materials (mmol/L)	145 NaCl	30 NH_4Cl	0 Na	Na and HCO_3^-	0 Na and HCO_3^-	0 Na and 20 NH_4Cl	Nigericin
NaCl	145	115	-	125	-	-	10
KCl	4	4	4	4	4	4	120
$CaCl_2$	1.5	1.5	1.5	1.5	1.5	1.5	1.5
$MgSO_4$	1	1	1	1	1	1	1
$NaHCO_3$	-	-	-	22	-	-	-
Glucose	5	5	5	5	5	5	5
HEPES	10	10	10	-	-	-	10
Choline-HCO_3	-	-	-	-	22	-	-
NMDG-Cl	-	-	125	-	110	125	-
NH_4Cl	-	30	-	-	-	20	-
Nigericin	-	-	-	-	-	-	0.01

RESULTS

Tg737^{orpk} mutant mice exhibit hydrocephalus

The *Tg737^{orpk}* hypomorphic mutant mice are severely growth retarded and normally die within the first few weeks of birth due to pathologies in multiple tissues, including hydrocephalus. The hydrocephalus phenotype in these mice is evident shortly after birth with an enlarged cranium. The gross appearance of the brain shows minor compression of the olfactory bulbs and cerebellum suggestive of increased intracranial pressure. Histological analysis indicates that the lateral ventricles are enlarged in mutants relative to the wild-type controls (Figure 8).

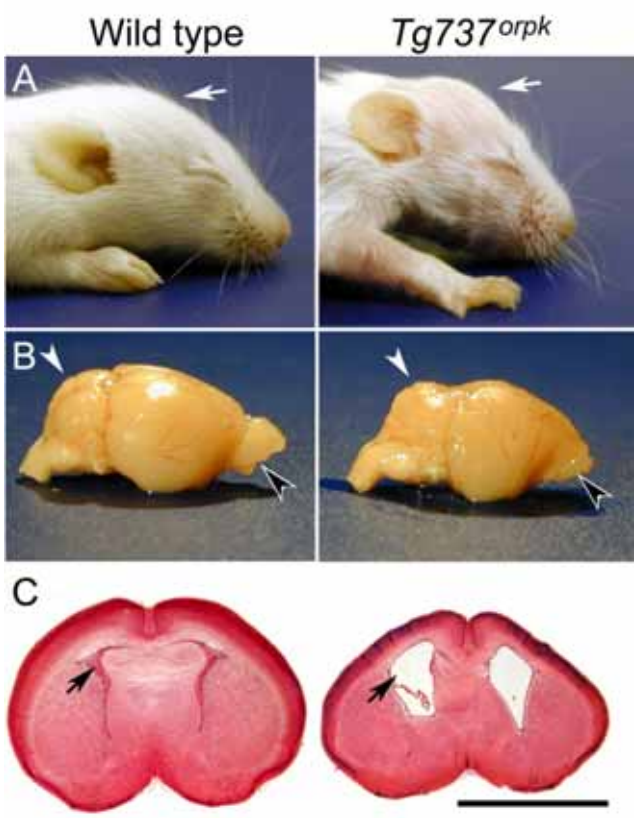

Figure 8. *Tg737^{orpk}* mutant mice develop hydrocephalus. (A) Comparison of lateral view of 10-day-old wild-type and *Tg737^{orpk}* mice indicates that the mutants exhibit a bulging forehead (arrow), characteristic of hydrocephalus. (B) Gross analysis of the brains from mutants shows signs of compression at the olfactory bulb and the frontal pole of the cerebrum (black arrowhead). Also, the cerebellum is more prominent in mutant animals (white arrowhead) than in wild-type control. (C) Hematoxylin and eosin stained coronal sections of the brain through identical regions of the brain demonstrate marked dilatation of the lateral ventricles in mutant animals compared to wild-type controls. Scale bar is 4 mm.

Initiation and progression of the hydrocephalus in Tg737^{orpk} mutant mice

To follow progression of hydrocephalus *in vivo,* we analyzed the phenotype of four pairs of mutant and wild-type littermates at postnatal day 1 and again at day 6 using T2 RARE magnetic resonance imaging (MRI). Coronal MRI sections of day 1 mutant brains exhibit larger fluid-filled lateral ventricles compared to their wild-type littermates (Figure 9). Analysis of the same mutants at day 6 indicates that the lateral ventricles become even larger while the wild-type lateral ventricles are small and difficult to distinguish from the surrounding brain tissue. The same results were seen from the paramedian sagittal view. Median-sagittal images were used to obtain information about the third ventricle-aqueduct-fourth ventricle axis which is the narrowest portion of the entire ventricular system and its obstruction is the most frequent cause of hydrocephalus. Median-sagittal sections of 1-day-old wild-type and mutant littermates reveal no overt morphological difference in this axis. By day 6, the protrusion of the cerebellum into the cisterna magna and the skull protuberance above the cerebellum indicate that increased intracranial pressure may be present in these animals, suggestive of duct obstruction. However, the resolution of the MRI images was not sufficient to establish whether the aqueduct in the mutants was open or obstructed at these stages. Therefore, this was further addressed by intra-ventricular injection of DiI (see below). The analysis of the MRI images indicated that the normalized ventricular volume was 3.1-fold and 5.3-fold higher in mutants than in wild-type controls at day 1 and 6, respectively. Thus, by day 1 there was already a significant increase in the ventricular volume.

In contrast to the ventricular data, MRI analysis did not show alterations in the subarachnoid space, suggesting that there are no overt defects in CSF reabsorption.

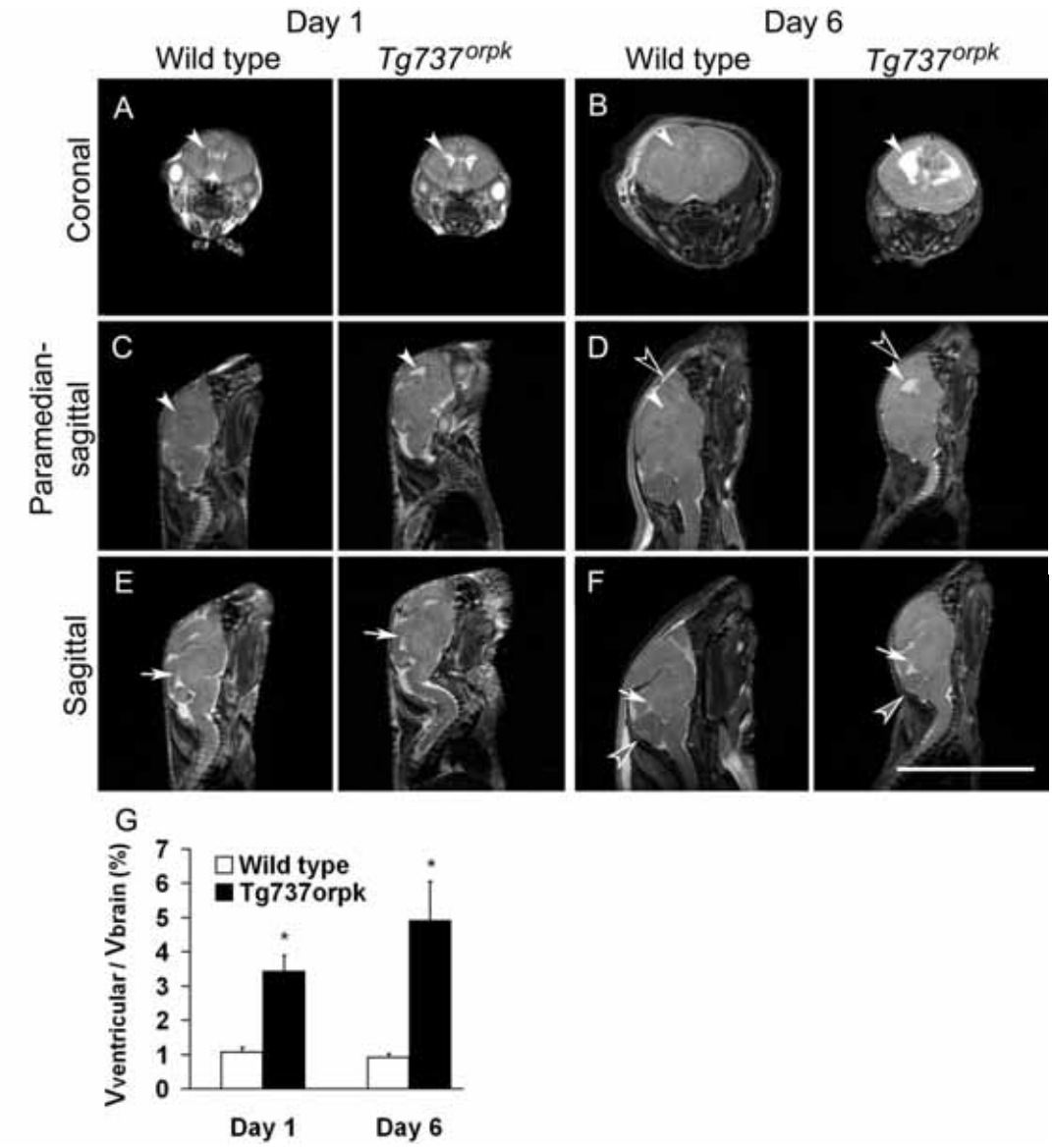

Figure 9**.** Analysis of hydrocephalus progression in *Tg737*^{orpk} mutant mice using T2 RARE MRI. Compartments containing CSF appear white while brain matter is gray. (A-B) Dilatation is evident in the lateral ventricles (white arrowheads) of one-day-old mutants as compared to wild-types. (C) In contrast, there is no sign of expansion in the fourth ventricle or in the aqueduct (arrows) at this age. (D-E) By day 6, the lateral ventricles of the mutants are markedly enlarged (white arrowheads), without overt differences in the (F) fourth ventricle and aqueduct but protuberance is seen on the skull above the cerebellum (gray arrowheads). (E) In the subarachnoid space no difference is detected between wild-type and mutant animals (black arrowheads). Scale bar indicates 10 mm. (G) Quantitative measurement of the relative ventricular volume in the mutant and wild-type controls at each age (n = 4; **P* < 0.05).

Cilia are malformed on Tg737^{orpk} mutant ependymal and choroid plexus epithelia

Previous data indicated that polaris and its homologs in *Chlamydomonas* (IFT88) and *C. elegans* (OSM-5) function as an IFT particle protein required for cilia formation (26, 44). Inside the ventricular system, cilia are found on ependymal cells which line the ventricles as well as on CP epithelia. While the importance of the cilia on the CP has not been explored, beating of the numerous motile cilia on ependymal cells is thought to facilitate CSF movement and data indicate that loss of these cilia is associated with severe hydrocephalus. Thus, to further explore a connection between the pathogenesis of hydrocephalus and cilia defects in *Tg737^{orpk}* mutants, we compared the cilia on the ependyma and CP epithelia in mutant and wild-type mice by immunofluorescence and by scanning electron microscopy.

The ependymal cells of adult mice have numerous long cilia that extend into the ventricular lumen. On wild-type CP epithelium, most cells have a small tuft of cilia on the apical surface; however, there were also numerous CP cells with a single primary cilium. The functional importance of either of these cilia types is unknown (Figure 10).

In agreement with the hypomorphic nature of the *Tg737^{orpk}* mutation, polaris expression and cilia were still detected on the ependyma and CP epithelium of mutant animals. Compared to wild type controls, the cilia on the mutant ependyma were fewer in number, disorganized, stunted, anisometric, and often exhibited a bulb-like structure at their tips in which the mutant form of the polaris protein accumulated (Figure 10). These bulb-like structures were also observed on the CP epithelia and as seen on the ependyma, the mutant form of polaris was concentrated at the tip. These morphological differences were also evident using scanning electron microscopy and are in agreement with recently published data showing that primary cilia on renal collecting duct cells of *Tg737^{orpk}* mutants also have this bulb-like structure (37).

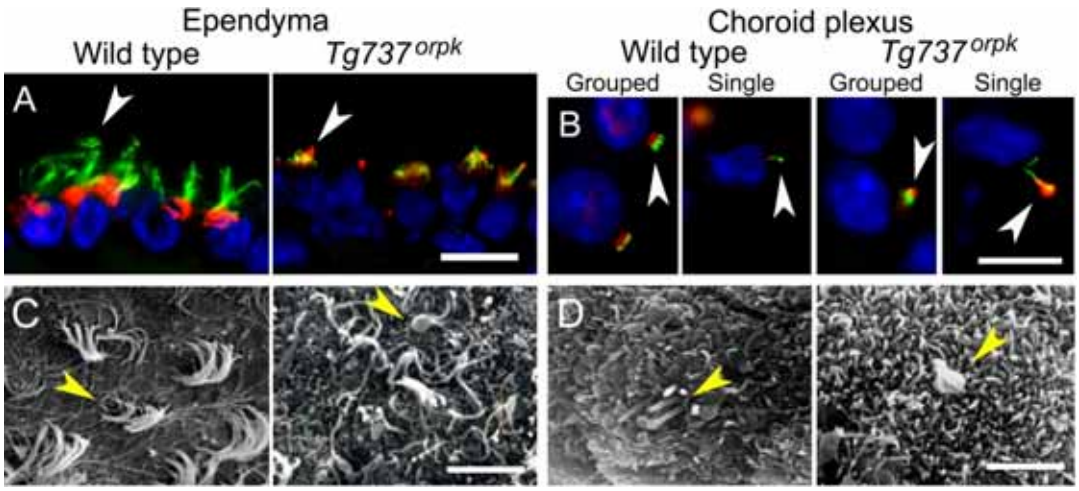

Figure. 10. Altered cilia morphology on cells of the ventricular system in *Tg737*^{orpk} mutant mice. Photomicrographs of brain sections from wild-type and mutant animals showing immunolocalization of acetylated-α-tubulin (green) and polaris (red). White and yellow arrowheads point to cilia. (A) Ependymal cilia in wild-type mice are in well-organized groups with equal length while cilia on the *Tg737*^{orpk} mutant ependyma are fewer in number, shorter and anisometric. Polaris predominantly localizes to the basal body in the wild-type ependyma, while polaris is found to accumulate at the cilia tip in the mutants. (B) Grouped and primary cilia are present on the CP of wild-type mice and polaris is concentrated at the basal bodies. Polaris accumulates at the tip of the grouped and primary cilia in *Tg737*^{orpk} mice. Cilia often exhibit a large bulb-like structure in which polaris is concentrated. (C) Scanning electron microscopy (SEM) of ependymal cilia of normal and *Tg737*^{orpk} mutant mice (D) Cilia on CP of normal and *Tg737*^{orpk} mutants. In mutants, the cilia are morphologically abnormal with a thickened axoneme. Scale bars on immunofluorescence and SEM images represent (A) 20, (B) 10, (C) 15 and (D) 2.5 μm, respectively.

Malformed cilia in Tg737*^{orpk} *mutants results in impaired beat and reduced fluid flow

The cilia morphology defects on the ependymal cells of *Tg737*^{orpk} mutants suggest that hydrocephalus may be associated with altered cilia beat and subsequently impaired CSF movement. To assess these possibilities, we analyzed cilia beating on freshly isolated ependymal cells using time-lapse DIC and fluorescence microscopy with small fluorescent beads added to track fluid movement (see movie in supplementary data). On wild-type ependyma, cilia beat was rapid, well orchestrated, and produced a laminar flow across the cells. In contrast, the movement of cilia on mutant ependyma exhibited a low frequency beat, which was asynchronous and failed to produce significant amount of directional fluid flow (Figure 11). Thus, as seen for

other mouse mutants, defects in the cilia motility in the *Tg737*^{orpk} mutants is consistent with impaired CSF flow through the ventricles and with the development of hydrocephalus (28).

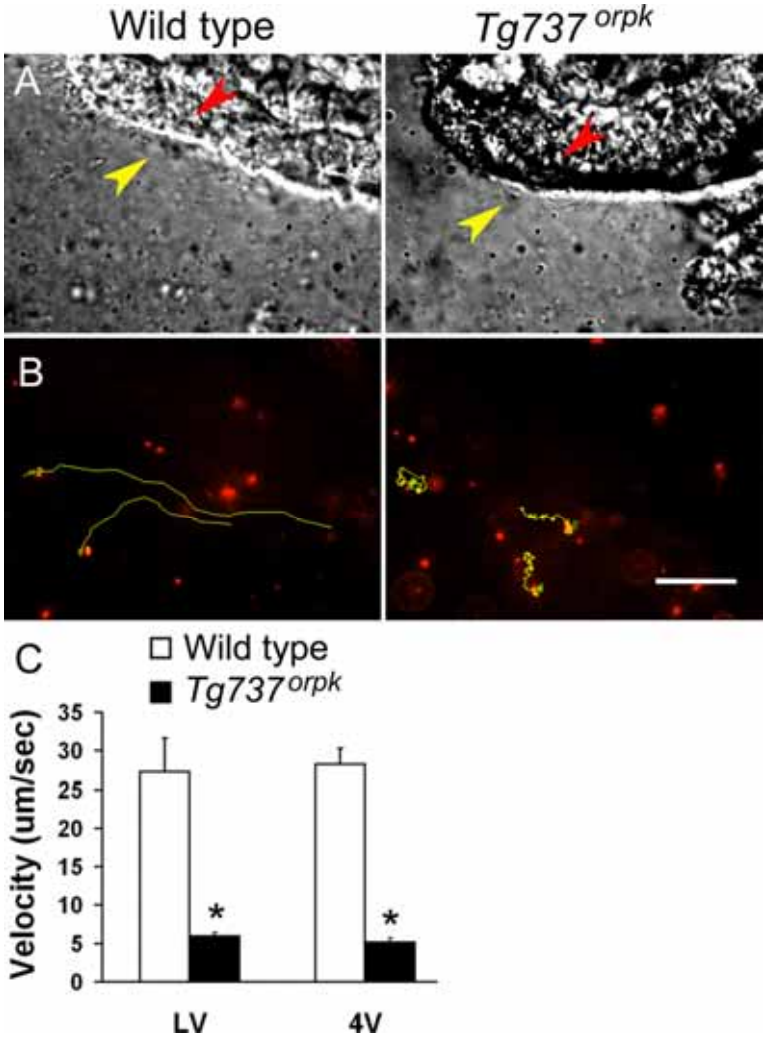

Figure. 11. Defects in cilia beat of the *Tg737*^{orpk} mutant results in impaired fluid flow over the ependymal cells. Red and yellow arrowheads label ependyma and ependymal apical cilia, respectively. (A) DIC and (B) fluorescence images of wild-type and mutant ependyma. Fluorescence images were overlaid with the movement of the fluorescently labeled beads as recorded by motion tracking (yellow lines, see supplemental movie). Movement of beads propelled by wild-type cilia beating is rapid and directional while beads moved randomly in the mutant samples. Scale bar is 20 μm. (C) Graph showing quantitative analysis of the flow generated by the cilia from mutant and wild-type samples (n=6; **P*<0.005).

The hydrocephalus in Tg737^{orpk} mutants precedes formation of motile cilia on ependymal cells

To further evaluate a connection between cilia defects, impaired CSF flow, and the etiology of hydrocephalus, we analyzed when and where motile cilia first become evident on cells in the ventricular system of wild-type mice and correlated these data with the appearance of hydrocephalus in the *Tg737^{orpk}* mutants.

Our analysis of cilia formation on ependymal cells using serial section immunofluorescence indicated that in one-day-old wild-type mice, most ependymal cells lining the ventricles had only a primary cilium. The presence of the multi-ciliated cells did not occur on the ventricular walls until around postnatal day 7. This was well after the pathology develops in the *Tg737^{orpk}* mutants (postnatal day 1), suggesting that loss of these motile cilia and subsequent flow generated by them cannot be the cause of the hydrocephalus. One exception to this was the cells lining the aqueduct interconnecting the third and fourth ventricle. Most of these cells were multi-ciliated by postnatal day one (Figure 12). Thus, the loss of motile cilia in the aqueduct of mutants could impair flow through the duct and lead to pathology similar to obstructive hydrocephalus.

In contrast to the ependymal cells, the cilia on wild-type CP epithelium were well formed by day 1 and were similar to that seen in the adults. Since these cilia are present when hydrocephalus initiates, loss of their function could contribute to the pathology. While cilia on the multi-ciliated CP epithelium are motile (data not shown), our analyses indicate that they would have minimal effect on generating CSF flow.

Initiation of hydrocephalus in Tg737^{orpk} mice occurs prior to aqueduct stenosis

In contrast to the ependymal cells lining the ventricular walls, motile cilia were present on aqueduct cells prior to the onset of hydrocephalus, raising the possibility that impaired function of these cilia may initiate the phenotype. This could occur by duct stenosis which is normally inhibited by the beating of the cilia on these cells or by impaired CSF flow through these narrow structures in the absence of normal cilia beat.

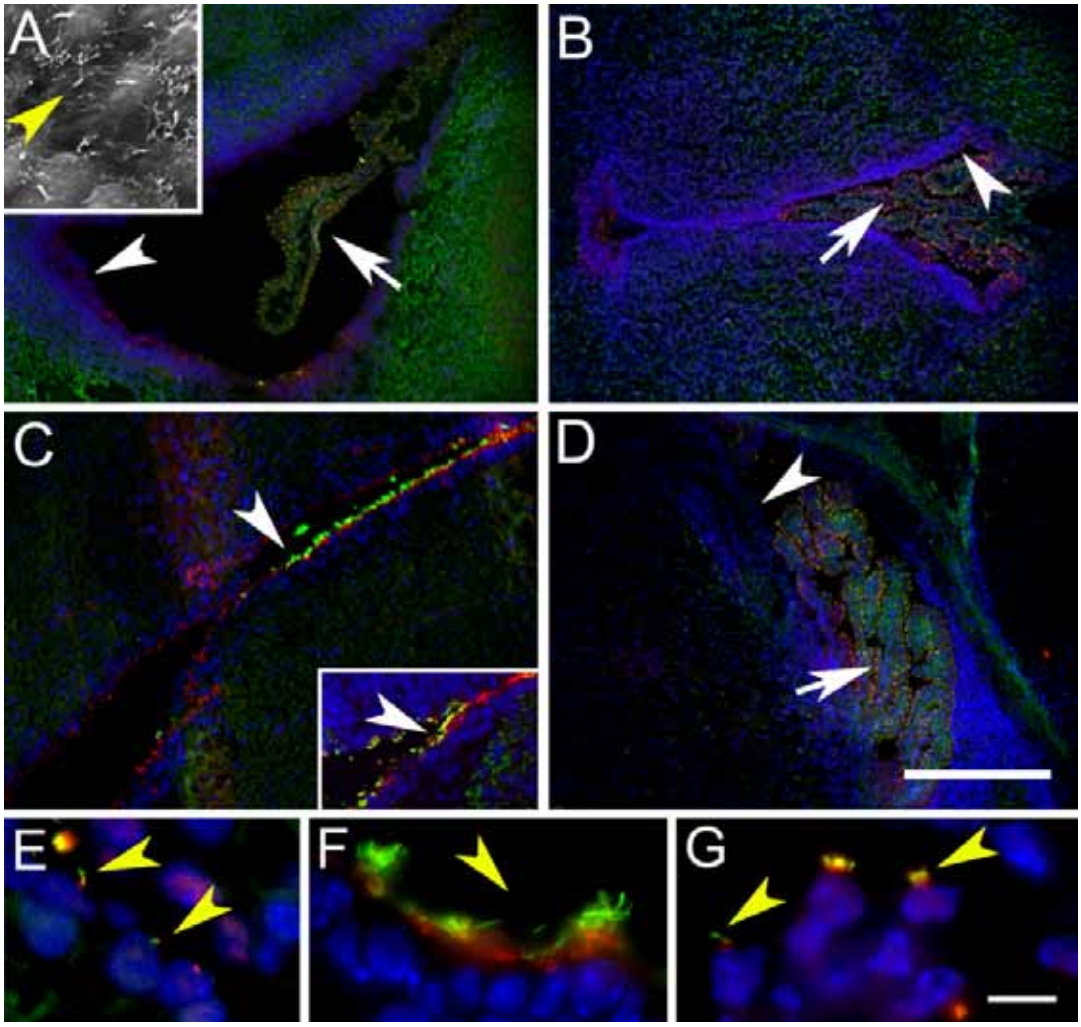

Figure 12. Analysis of cilia in the ventricular system in one-day-old mice. Brain sections of a one-day-old wild-type mouse containing the (A) lateral, (B) third ventricles, (C) the aqueduct, and (D) the fourth ventricle were analyzed for the presence of cilia (anti-acetylated-tubulin, green and polaris, red) on the ependyma (white arrowheads) and choroid plexus epithelia (white arrow). No multi-ciliated cells were evident on the ependyma of the (A) lateral, (B) third or (D) fourth ventricles at this age. Ependymal cells possess primary cilium as shown with the SEM and immunofluorescence (insert in A and E, yellow arrowheads). (C) In contrast, the ependymal lining of the aqueduct was multi-ciliated (white arrowhead). Inset shows that multiple cilia are also present in the mutant aqueduct. (F) Multiple cilia cover cells in the aqueduct (yellow arrowheads). (G) Grouped and single cilia on the choroid plexus . Scale bars equal to 200 μm and 10 μm on panels (A to D) and (E to G), respectively.

To begin testing these possibilities, CSF flow was evaluated using fluorescent dye DiI injected into one lateral ventricle of day 2 and day 6 wild-type and *Tg737^{orpk}* mutant mice. The movement of DiI through the ventricles was analyzed by serial sectioning of the brain. To initiate this analysis, we evaluated DiI movement in wild type (day 2 and 6) mice at 5, 10, 20, and 30 minutes after injection into the lateral ventricle to determine the time needed for it to be detected in the fourth ventricle. DiI was detected at all time points except at 5 minutes, thus all subsequent analyses were performed after 10 minutes (Figure 13). Our analysis of day 2 mutants was indistinguishable from the wild type controls. This confirms that the aqueduct remains patent in the early stages of the disease and that impaired motility of the cilia lining the aqueduct at this early age does not result in obstructed CSF flow that could cause the pathology. In contrast to the two-day-old mutants, in six-day-old *Tg737^{orpk}* mice DiI was not detected in the fourth ventricle indicating that passage through the aqueduct had been compromised. Since this occurs late in the pathogenesis of the disease in these mutants, duct stenosis and loss of flow is likely a consequence rather than a cause of hydrocephalus.

Cell polarity on the choroid plexus epithelia of Tg737^{orpk} mutants.

Another potential pathogenic mechanism is altered cell polarity, similar to that seen for the kidney of *Tg737^{orpk}* mice as well as several other PKD mouse models, which have revealed mislocalization of polarized proteins such as the EGF receptor and Na^+/K^+-ATPase (74). In the kidney, this results in excess fluid accumulation in the tubules and the development of the cystic pathology (3, 74). Here, we analyzed sections of brains for the localization of α-catenin and ZO-1 , indicators of general polarity as well as transport proteins such as the Na^+/K^+-ATPase and the anion exchanger 2 (Figure 14). The data indicate that all these proteins were localized normally in the mutants and at similar levels when compared to the control samples. Thus, there were no overt defects in the organization of the tissue due to defects of the cilia.

Another aspect of polarity that we analyzed was whether distribution of signaling proteins in the cilia axoneme was affected. Altered localization of proteins in the axoneme could lead to their dysfunction and impair the sensory or signaling activity

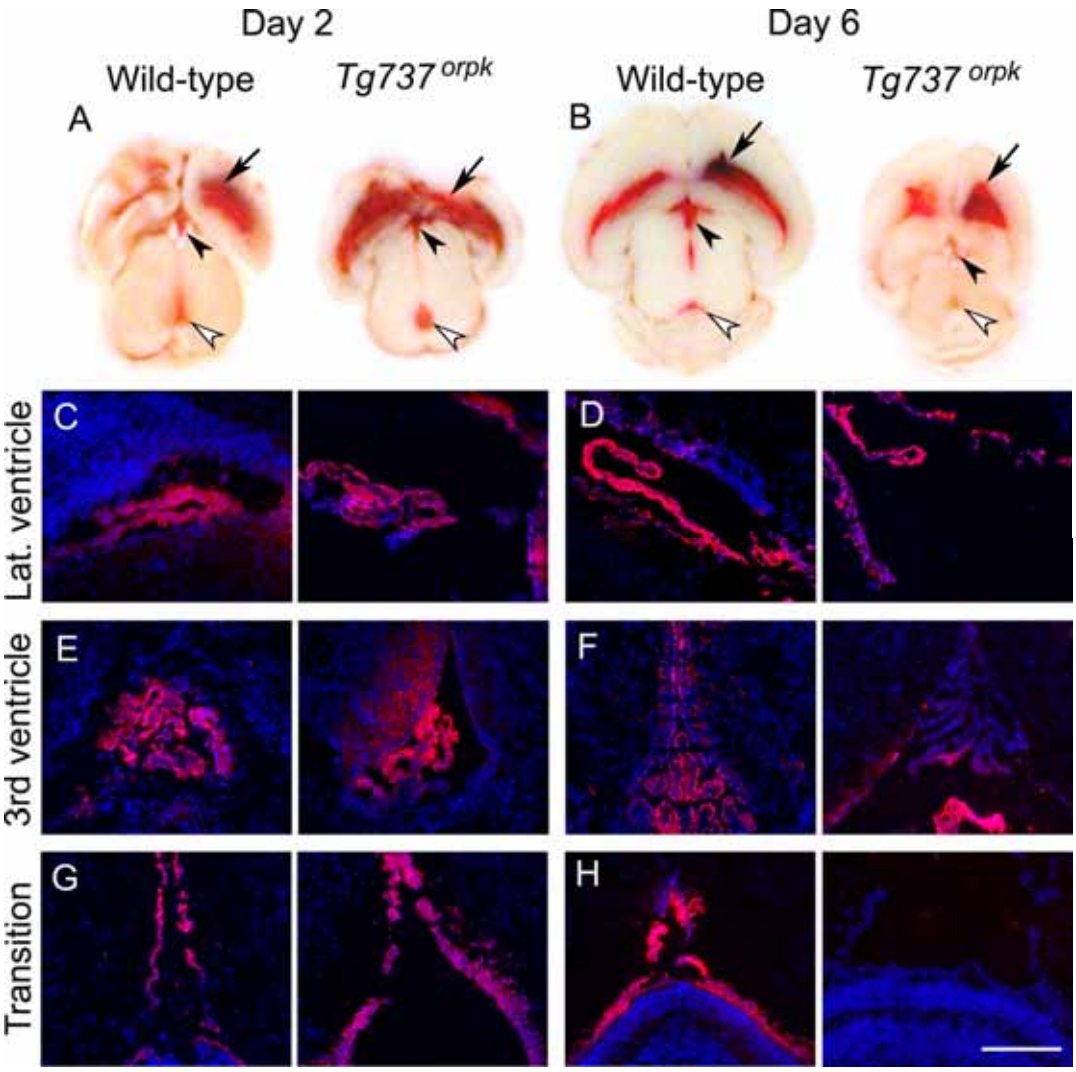

Figure 13. The initiation of hydrocephalus precedes aqueduct stenosis in *Tg737*^{orpk} mutant mice. Movement of the DiI (red) was tracked through brain sections of two and six-day-old wild-type and *Tg737*^{orpk} mutant mice 10 minutes postinjection. (A and B) Horizontal view of brains showing the lateral ventricles (black arrows), third ventricle (black arrowheads) and fourth ventricle (white arrowheads). (C-H) Fluorescence images of brain sections through the indicated regions from (C, E and G) 2-day-old and (D, F and H) 6-day-old control and mutant mice. DiI is detectable in the fourth ventricle of 2-day-old mutants (A and G, right panels) but is not seen in 6-day-old mutants (B and H, right panels), indicating that CSF movement was obstructed in these mutants. Scale bar represents 200 μm.

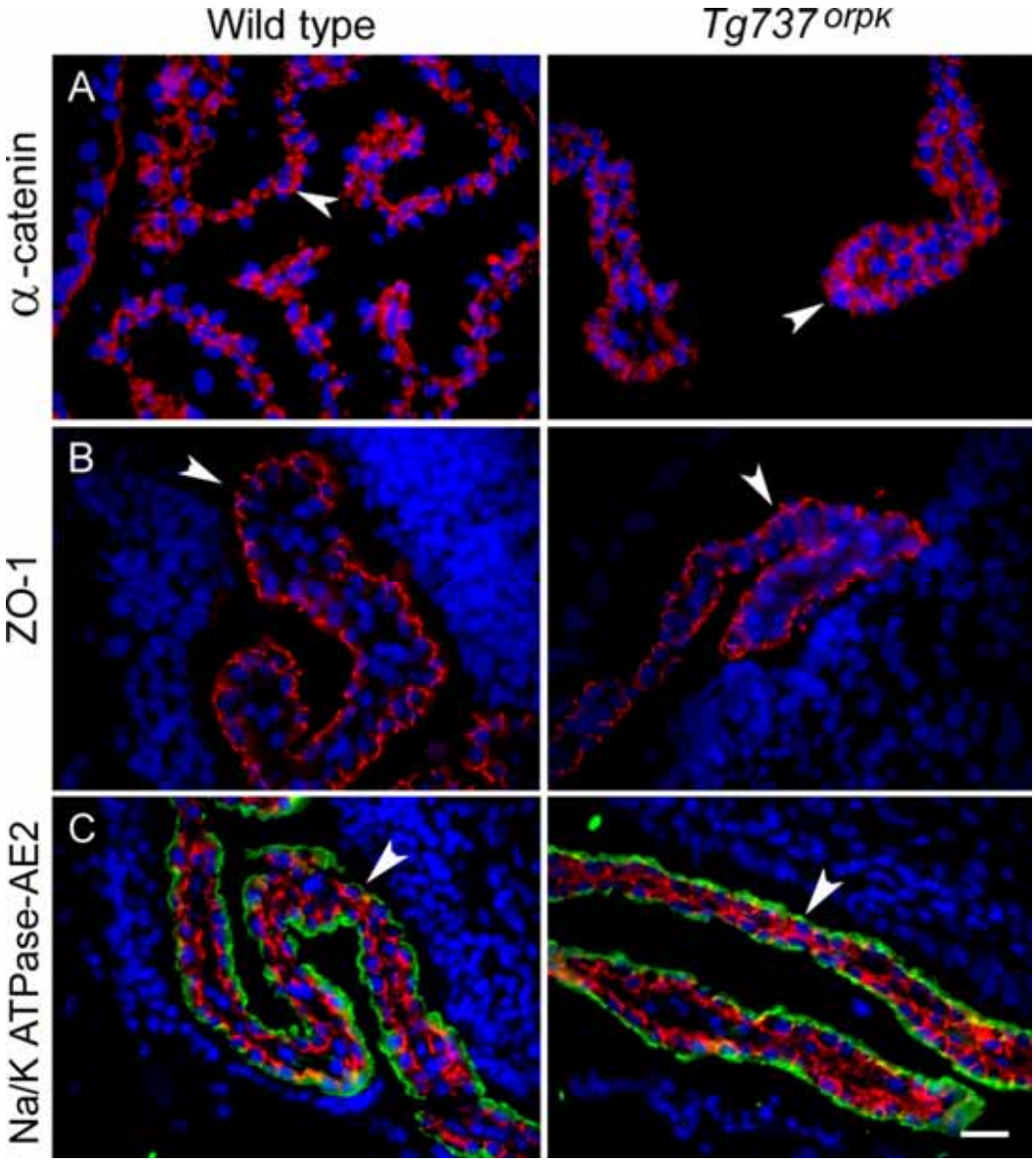

Figure. 14. *Tg737*^{orpk} mutant mice demonstrate no overt loss of epithelial polarity in the choroid plexus. Arrowheads indicate the apical surface of choroid plexus. (A) Expression of α-catenin (red) in sections of wild-type and mutant mice. (B) ZO-1 (red) is localized to the tight junctional complexes near the apical surface of wild-type and mutant choroid epithelia. (C) Analysis of transport proteins Na^+/K^+ATPase (green) and the anion exchanger type 2 (AE2, red) show normal localization at the apical and basolateral membranes, respectively. Scale bar is 20 μm.

of these cilia as proposed in the kidneys of cystic mutants. Since there are no data with regards to signaling proteins in the cilia of the CP, based on previous studies of the renal cilia, we evaluated whether polycystin-1 was present in the cilia of the CP and whether its distribution was affected by the *Tg737* mutation. Polycystin-1 is an integral cilia membrane protein involved in a fluid flow induced calcium signaling pathway (42, 46). As seen in primary cilia of the kidney, polycystin-1 localized predominantly at the basal bodies in both multi and primary ciliated cells and at lower levels along the cilia axoneme in wild-type CP (Figure 15). In contrast, in *Tg737*^{orpk} mutants polycystin-1 was concentrated in the bulb-like structure at the tip of cilia in CP, rather than the basal body. While polycystin-1 mutations are not associated with hydrocephalus, this example supports the possibility that there may be cilia mediated signaling defects in the CP of the *Tg737*^{orpk} mutants resulting from mislocalization of cilia proteins in the axoneme or in the subsequent transmission of a signal from the cilia into the cell as proposed for cystic kidney disease (64).

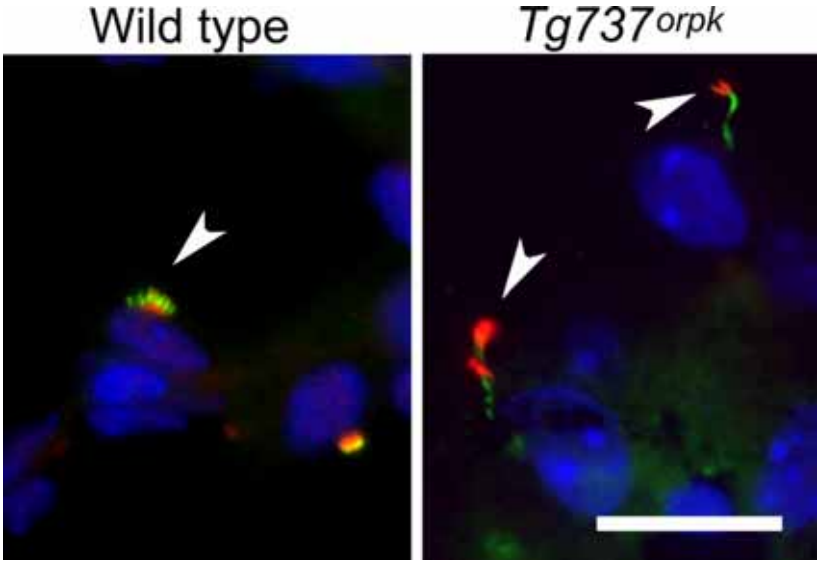

Figure. 15. Altered localization of proteins in the cilial axoneme of *Tg737*^{orpk} mutants. On wild-type choroid plexus, polycystin-1 (red) was localized predominantly to the base of the cilia (acetylated-α-tubulin, green), while in the mutants, polycystin-1 accumulated in the bulb-like structures at the cilia tip. Scale bar represents 20 μm.

Analysis of proliferation in choroid plexus epithelium of Tg737^{orpk} mutants.

There are several models of hydrocephalus where pathogenesis is associated with excess CSF production due to hyperproliferation of CP cells (i.e. CP papillomas). In addition, a hallmark of cystic kidney disease is increased proliferation of the cystic epithelium. To determine if increased CP cell number is associated with the pathology, we evaluated whether proliferation was altered in the CP of *Tg737^{orpk}* mutants. The data indicate that there are no significant differences in proliferation in the CP of the *Tg737^{orpk}* mutants (Table 2).

Table 2**.** Cell proliferation in the CP of *Tg737^{orpk}* mutant mice

Mice	**Proliferation index positive nuclei/nuclei**
Wild-type	$(3.75 \pm 0.31) \times 10^{-3}$
Tg737^{orpk} mutant	$(4.175 \pm 0.36) \times 10^{-3}$ n.s.

Comparison of mean ± SE values for positive cells (positive nuclei/nuclei) of mutant (n = 5; n.s.: non significantly different from wild-type control).

Tg737^{orpk} mutants have increased intracellular cAMP levels in the choroid plexus and elevated chloride concentration in the CSF.

An alternative mechanism associated with the development of hydrocephalus could be elevated CSF production. Nearly all CSF is produced by the CP through directional transport of chloride and bicarbonate to the ventricular lumen (apical) (10). Thus, to determine whether cilia dysfunction may have an effect on CSF production, we compared chloride concentration in CSF isolated from mutant and wild-type mice. The chloride level was significantly higher in mutant CSF relative to wild-type controls (Figure 16).

Chloride transport into the CSF is regulated in part by an apically localized inward-rectifying chloride channel which is activated by intracellular cyclic AMP (cAMP) signaling (10, 32). To investigate a possible mechanism leading to elevated chloride in mutant CSF, we measured the intracellular concentrations of cAMP in CP cells freshly isolated from five-day-old mutant and wild-type mice. In support for elevated chloride secretion by the CP, the intracellular levels of cAMP were significantly increased in mutant animals compared to the wild-type (Figure 16).

Together these data suggest that loss of normal cilia function on the CP results in aberrant cAMP regulated chloride transport that would lead to enhanced fluid movement into the ventricle lumen and to excess CSF production.

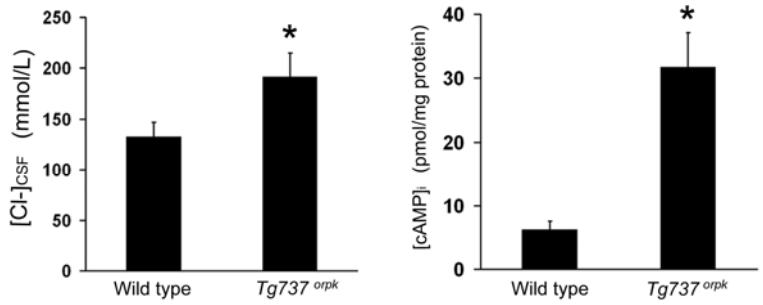

Figure. 16. Choroid plexus physiology is altered in the *Tg737*^{orpk} mutants. Graphs indicating the (A) chloride concentration in the cerebrospinal fluid of wild type and mutant mice. (B) Intracellular cyclic AMP level ($[cAMP]_i$) in the CP epithelium from wild-type and mutant animals (n=6 and n=7; **P*< 0.05 and **P*< 0.005, respectively).

Technique of simultaneous imaging of paired tissue preparations

Analysis of physiological parameters, such as pH_i, can have a high degree of experimental variability as a result of the assay procedures. This can make it difficult to assess the physiological significance of changes that result from experimental or genetic manipulations. Thus, we utilized a simultaneous imaging approach (presented in Figure 17) to directly compare pH_i and Na^+-dependent transport activities in *Tg737*^{orpk} mutant and wild-type choroid plexus epithelium. With this technique, the choroid plexi from two groups of animals (e.g. wild-type and *Tg737*^{orpk}) are simultaneously loaded, incubated, and imaged. This eliminates variability conferred by experiment-to-experiment differences due to loading conditions and timing of solution changes, etc, and allows a more direct comparison of data between samples.

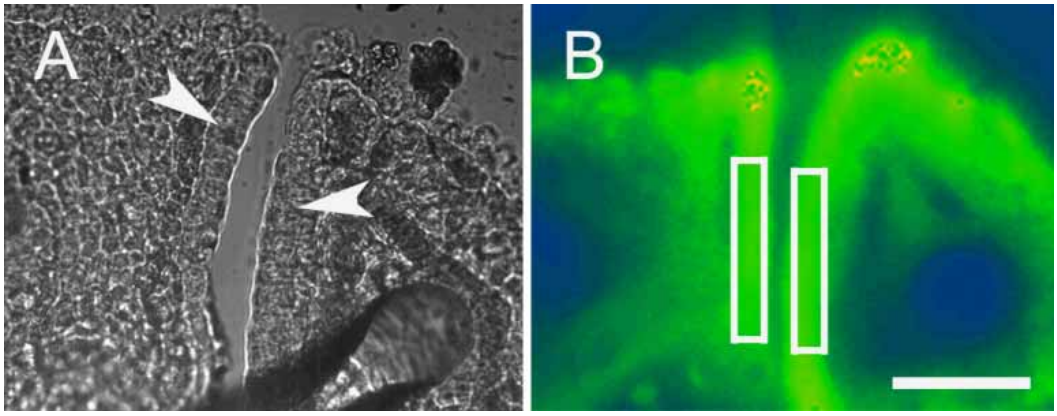

Figure 17. Freshly isolated *in vitro* choroid plexus preparations from wild-type and *Tg737*^{orpk} mutant mice visualized simultaneously in one image field. (A) Bright-field image showing the wild-type and mutant choroid plexus tissues immobilized by micropipettes. Arrowheads indicate the epithelial cells at the edge of the choroid plexus. (B) Wide-field fluorescence image of the same tissues loaded with the intracellular pH sensitive dye BCECF. White rectangles represent the regions of interest corresponding to the epithelial cells. Scale bar denotes 40 μm.

Steady-state pH_i in choroid plexus epithelia from wild-type and Tg737^{orpk} mice in the presence or absence of CO_2/HCO_3^-

Baseline pH_i is determined by the balance between acid-loading mechanisms (acid loading transporters and passive fluxes of acid-base equivalents) and acid-extruding mechanisms (acid-extruding transporters). The activity and expression of many of the acid-base transporters are regulated by intracellular cAMP (24, 25, 59). Thus, we first investigated the pH_i in choroid plexus epithelium from mutant and wild-type mice. As shown in Figure 18, the steady-state pH_i was found to be higher in CO_2/HCO_3^--buffered solutions than in HEPES-buffered solutions, and under both conditions, pH_i was significantly lower in choroid plexus epithelium obtained from *Tg737*^{orpk} mutants than from wild-type animals.

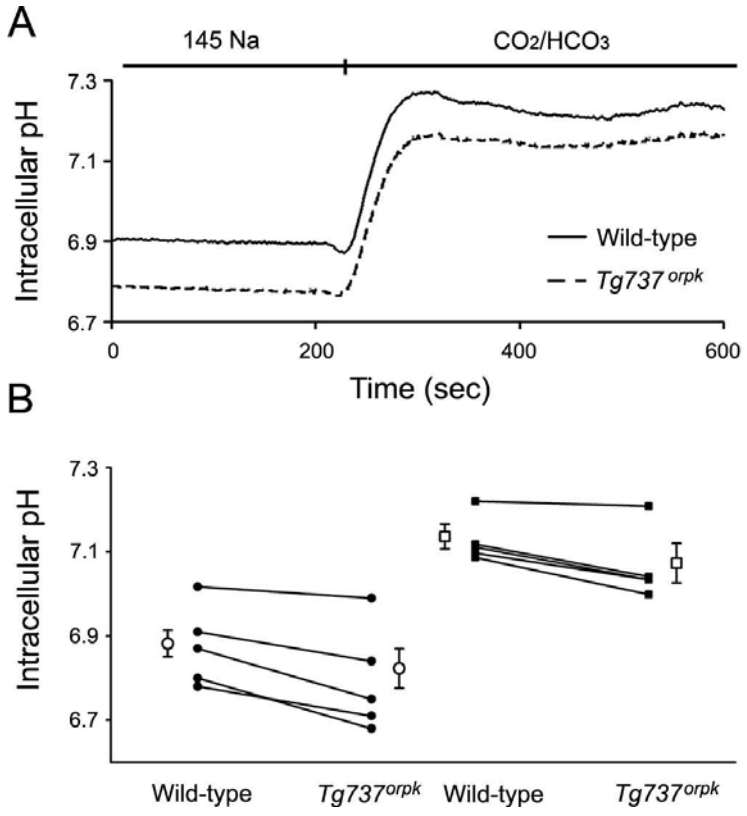

Figure 18. Measurement of intracellular pH in choroid plexus epithelia. (A) Representative traces demonstrating steady-state pH_i in choroid plexus epithelia from simultaneously imaged wild-type and *Tg737*^{orpk} mutant tissues in the absence or presence of CO_2/HCO_3^- in the bath. (B) Graphs showing pH_i values in CP epithelia in the absence (circles) or presence (squares) of CO_2/HCO_3^- from wild-type and mutant animals. Filled symbols denote pH_i values from individual paired preparations, and open symbols show the average values ± SE (n=5; the values in the wild-type and mutant groups were different from each other under both conditions).

Sodium-hydrogen antiporter activity in choroid plexus epithelia obtained from wild-type and mutant animals

The lower pH_i in choroid plexus epithelial cells from mutant animals relative to wild-types could be due to either stimulation of acid-loading or inhibition of acid-extruding mechanisms. Na^+-H^+ antiporter is a potent acid-extruder involved in regulating pH_i and maintaining cell volume in many tissues (6, 23, 51). We therefore examined Na^+-H^+

antiporter activity in both mutant and wild-type CP epithelial tissues (Figure 19). Tissues in the nominal absence of CO_2/HCO_3^- were first acidified using the NH_4^+-prepulse technique, and pH_i recovery was blocked by removing external Na^+. Na^+ was then readded and the initial rate of pH_i recovery was used as an index of Na^+-H^+ antiporter activity. Neither the wild-type nor the mutant CP epithelial tissues showed appreciable increase in pH_i upon returning Na^+ to acid-loaded tissues. Together these data suggest that altered pH_i is not due to defects of Na^+-H^+ antiporter activity.

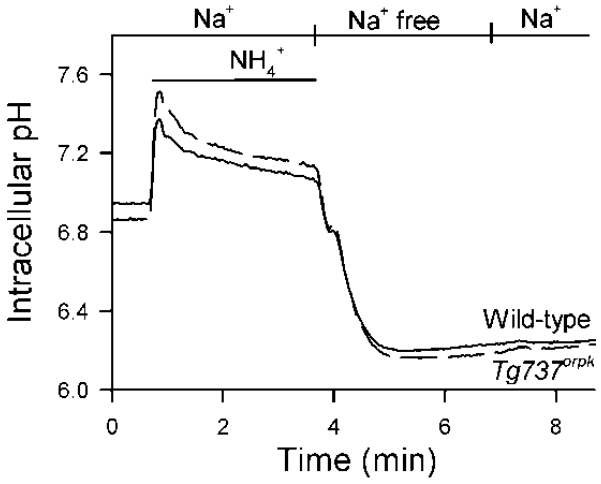

Figure 19. Dependence of pH_i on extracellular Na^+ in choroid plexus epithelia following an acid load in the absence of CO_2/HCO_3^-. Representative traces of Na^+-dependent pH_i recoveries following an intracellular acidification imposed by prior Na^+ removal for wild-type (solid line) and *Tg737^{orpk}* (dashed line) choroid plexus tissues.

Na^+-HCO_3^- cotransport in choroid plexus epithelia from wild-type and Tg737^{orpk} mice

Na^+-HCO_3^- cotransporters also play an important role in pH_i regulation (53). To date, three types of Na^+-dependent HCO_3^- transporters have been described in the choroid plexus epithelia. The two basolateral transporters - NCBE and NBCn1 - are suggested to play a role in Na^+ and HCO_3^- influx into the cells, while the apical NBCe2 may participate in the efflux of these ions to the cerebrospinal fluid, however the role of this latest transporter remains to be determined (8). We therefore compared the Na^+-

dependent HCO_3^- transporter activity in *Tg737*^{orpk} mutant and wild-type tissues. We used an acid-loading protocol similar to that described above. However, upon removing NH_4^+ and Na^+, we simultaneously switched to a solution buffered with 5% CO_2/22 mM HCO_3^- (Figure 20A). As shown in Figure 20B, the net acid extrusion (J_{net}) was significantly higher in the mutant CP epithelia as compared to wild-type. These J_{net} values primarily represent HCO_3^--dependent transport since there is very little Na^+-dependent pH_i recovery in the nominal absence of CO_2/ HCO_3^-.

The effect of DIDS on Na^+-dependent HCO_3^- transport was also determined. We used choroid plexus tissue dissected from the same animal and pretreated one sample with 500 μmol/L DIDS for 15 minutes. The Na^+-dependent HCO_3^- transport activity in DIDS-pretreated tissues was 87.3 % ± 19.2 % as compared to control (n=6).

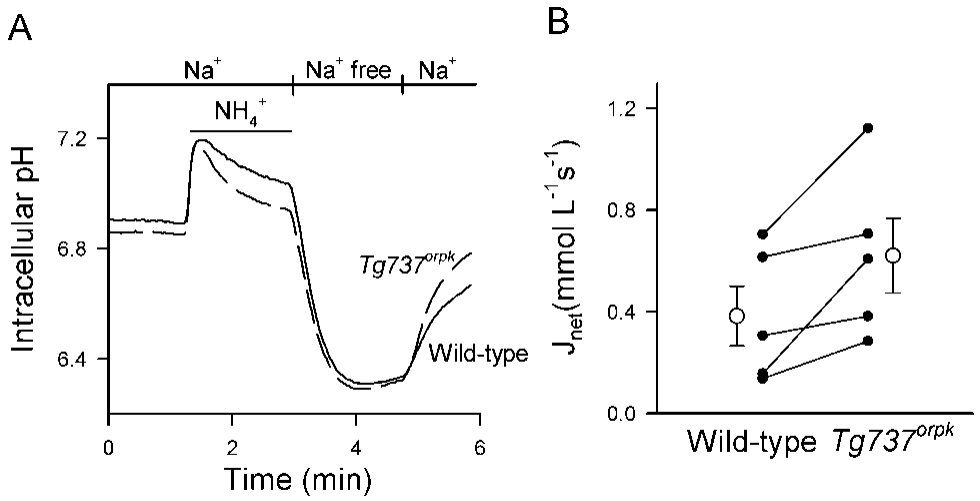

Figure 20. Dependence of pH_i on extracellular Na^+ in choroid plexus epithelia following acid load in the presence of CO_2/HCO_3^-. (A) Representative traces of Na^+-dependent pH_i recoveries following an intracellular acidification imposed by prior Na^+ removal for wild-type (solid line) and *Tg737*^{orpk} (dashed line) choroid plexus tissues. The initial rate of pH change was measured over 30 seconds. (B) Net Na^+-dependent acid extrusion flux (J_{net}) after an acid load in wild-type and *Tg737*^{orpk} choroid plexus tissues. Filled circles denote pH_i values from individual paired preparations, and open circles show the average values ± SE (n=5; the values in the wild-type and mutant groups were different from each other).

Effect of db-cAMP and H-89 on Na^+-dependent HCO_3^- cotransport in choroid plexus epithelium

An increased level of cAMP has been reported to activate Na^+-dependent HCO_3^- transport in pancreas, intestine and corneal epithelia (4, 67, 73). Also, as indicated above increased levels of cAMP were found in *Tg737^{orpk}* CP epithelia. Thus, we tested the possibility that an increase in intracellular cAMP could stimulate Na^+-dependent HCO_3^- transport activity in CP epithelial tissue from wild type mice similar to that seen in *Tg737^{orpk}* mutants. For this analysis, pairs of CP epithelial tissues were isolated from wild-type mice. To evaluate cAMP responses, one of the tissues was pretreated with 1 mM dibutyryl-cAMP for 20 minutes prior to the experiment and the Na^+-dependent HCO_3^- transport activity was compared to the control CP epithelia. As shown in Figure 21A and B, the Na^+-dependent HCO_3^- transporter activity was significantly higher in tissues pretreated with db-cAMP.

These data indicate that cAMP may be a modulator that leads to the altered Na^+-dependent HCO_3^- transport observed in the mutant CP epithelia. To further assess this possibility, we evaluated Na^+-dependent HCO_3^- transport activity in mutant CP epithelia under conditions where cAMP signaling was inhibited. This was done using H-89, a potent protein kinase A (PKA) inhibitor. As performed with the wild-type CP epithelial explants, a paired prep technique was utilized where one mutant sample was pretreated with H-89. In all samples analyzed, the preincubation with H-89 resulted in a significantly lower Na^+-dependent HCO_3^- transport activity as compared to the non-treated mutant tissue (Figure 21 C and D).

Together, these data support a mechanism by which loss of normal cilia function leads to elevated intracellular cAMP levels that cause defects in the regulation of Na^+-dependent HCO_3^- transport.

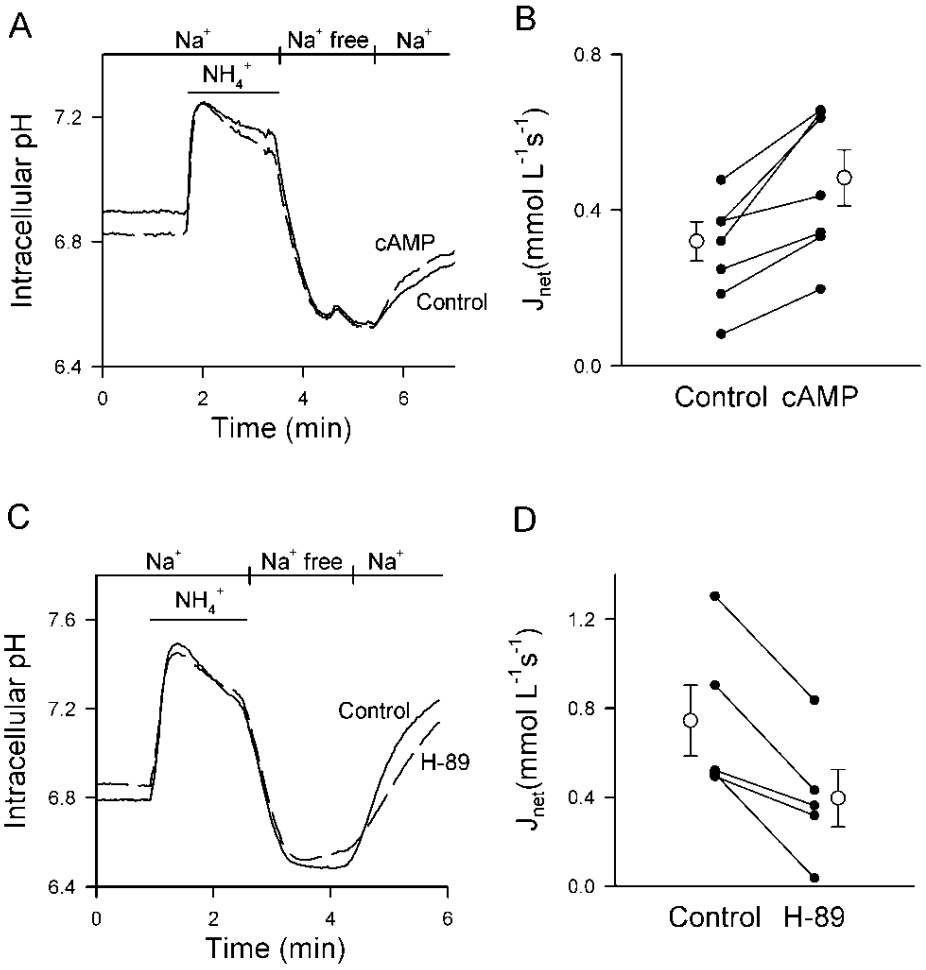

Figure 21. Effect of intracellular cAMP concentration on Na^+-dependent pH_i recovery after intracellular acidification in choroid plexus epithelia in the presence of CO_2/HCO_3^-. (A) Representative traces of Na^+-dependent pH_i recoveries following an intracellular acidification imposed by prior Na^+ removal for control wild-type (solid line) and db-cAMP treated wild-type (dashed line) choroid plexus tissues. The initial rate of pH change was measured over 30 seconds. (B) Net HCO_3^- flux after Na^+-addition in control and db-cAMP treated preparations (n=8; the values in the control and db-cAMP treated groups were statistically different from each other). (C) Representative traces of Na^+-dependent pH_i recoveries following an intracellular acidification imposed by prior Na^+ removal for non-treated *Tg737*^{orpk} mutant (solid line) and H-89 treated *Tg737*^{orpk} mutant (dashed line) choroid plexus tissues. (D) Net HCO_3^- flux after acid load in non-treated and H-89 treated *Tg737*^{orpk} mutant choroid plexus tissues. Filled circles denote pH_i values from individual paired preparations, and open circles show the average values ± SE (n=5; the treated and non-treated groups were statistically different from each other)

DISCUSSION

Hydrocephalus is a relatively common birth defect (11, 21). Despite the prevalence of this disorder and the existence of several genetic and induced models of the disease in mice and rats, our understanding of the molecular and cellular mechanisms causing the pathology has remained largely enigmatic. The proposed causes of hydrocephalus vary but they are all center on the net accumulation of CSF resulting from CSF overproduction, blocked CSF flow, or impaired CSF reabsorption. Due to our limited understanding of the causative mechanisms, current treatment strategies are palliative and rely on the insertion of shunts to drain excess CSF and reduce intracranial pressure and subsequent ventricular expansion.

In our work we utilized the *Tg737*^{orpk} hypomorphic mutants to further explore the connection between cilia and the development of hydrocephalus. MRI and histological analysis of the *Tg737*^{orpk} mutants indicate that the pathology is progressive and that it can be detected in the perinatal period. Since polaris is required for cilia assembly, we initially suspected that the hydrocephalus in the *Tg737*^{orpk} mutants would be associated with loss of motile cilia and subsequent impaired CSF flow as shown for other hydrocephalus mouse models (28, 69). Indeed, our analysis of the cilia in the *Tg737*^{orpk} mutants shows severe morphological abnormalities on the ependymal cells. This is similar to the pathogenic mechanism reported for the *Mdnah5* axonemal dynein mutant. In *Mdnah5* mutants, cilia on the ependymal cells form normally but are paralyzed and result in impaired CSF flow. This lack of CSF movement is thought to be an initiating factor leading to increased intracranial pressure, duct stenosis, and the development of hydrocephalus which becomes evident after postnatal day 6 (28).

In support of an impaired CSF flow mechanism, our *in vitro* analysis of the ciliary beat and fluid flow generated by the cilia on the ependymal cells isolated from the lateral ventricle of *Tg737*^{orpk} mutants revealed that the beat is disorganized and flow is impaired. However, when we correlated the time at which the pathology becomes evident (postnatal day one) in the *Tg737*^{orpk} mutants with when the motile cilia actually form on cells in the ventricles the data do not support a direct role for impaired cilia beat as being an initiating factor. An exception to this was the cells that line the

aqueduct interconnecting the third and fourth ventricles. Unlike the ependyma lining the ventricles, this ductal epithelium possesses motile cilia that are present prior to onset of the pathology. However, our *in vivo* analysis of CSF movement using DiI injection indicate no differences in CSF flow between the mutant and wild-type controls at early stages of the disease. Impaired CSF movement was evident only after significant expansion of the ventricles, suggesting that loss of CSF flow is a consequence of the pathology. These data raise the possibility that a mechanism other than duct obstruction or loss of CSF flow is the initiating factor leading to the development of hydrocephalus.

Another possible mechanism involves defects in the CP. The CP is a specialized secretory organ located within the brain ventricles and its primary functions are the production and homeostasis of the CSF (61). Our analysis of the CP cells indicate that there are two populations, one that has small tufts of motile cilia and another that has a single primary cilium. The function(s) of either of these types of cilia on the CP has not been explored. To our knowledge, this is the first description of primary cilia on the CP and we speculate that they have sensory roles similar to that shown in the embryonic node and in the renal tubules.

While not as common as obstructive hydrocephalus where CSF movement is impaired, communicative forms of this disease have also been described that result either from delayed reabsorption by arachnoid granulations or excess CSF accumulation, such as in the case of CP tumors. In most cases where there are defects in reabsorption, MRI analysis reveals an expansion in the subarachnoid space. This is not evident in the *Tg737*^{orpk} mutants suggesting that impaired reabsorption is not the cause. Since there is no overgrowth or increased proliferation of the CP in *Tg737*^{oprk} mutants, any effects on CP function would likely occur at the level of a pathway regulating secretory behavior of these cells. Thus, it is intriguing that our analysis of CSF composition indicates significant increase in the level of chloride. Chloride is transported through the activity of an unidentified apically localized inwardly rectifying chloride channel that is regulated by cAMP. Thus the increased chloride level in the CSF is supported by the elevated intracellular cAMP concentration in the CP epithelium. The elevated chloride level in the CSF suggests that the altered ion transport properties of the CP result in increased fluid movement and excess CSF production that would contribute to the development of hydrocephalus.

Intriguingly, in the *E2F-5* mutants, defects in CP secretory behavior are thought to cause a communicating form of hydrocephalus as seen in early *Tg737*^{orpk} mutants (36). This may be analogous to the mechanism of renal cyst development in mice and humans with cilia dysfunction (22). Several studies have shown that elevated cAMP signaling caused by the vasopressin receptor type 2 results in excess fluid secretion across cystic epithelium, and inhibition of which abrogates the cystic pathology. Thus it will be interesting to evaluate whether a similar mechanism is involved in the hydrocephalus pathology in *Tg737*^{orpk} mice (62, 70).

Summerizing the above discussed, the *Tg737*^{orpk} mice develop hydrocephalus that is initiated in the perinatal period and likely involves ion and fluid transport defects across the choroid plexus. This pathology was associated with a marked increase in intracellular cAMP. Another phenotype exhibited by the *Tg737*^{orpk} mutants is the development of cystic renal lesions in the kidney (40). While it is not known whether cAMP is elevated in the kidney of *Tg737*^{oprk} mutants, it is noteworthy that the cystic kidneys in human ARPKD and ADPKD patients and in many of the PKD mouse models caused by abnormal cilia function do have increased intracellular cAMP. Furthermore, inhibition of cAMP signaling using vasopressin receptor antagonists in mice with PKD greatly improves renal function and pathology and is currently being evaluated as a means of retarding cyst progression (70, 71, 72). Together, these data suggested that cAMP may be central to the initiation of hydrocephalus and other pathological alterations in the kidney, liver, and pancreas of the *Tg737*^{orpk} mutant mice.

cAMP is known to be an intracellular regulator of ion and water transport in many secretory/reabsorbtive epithelia (e.g. pancreas, intestine, cornea, and kidney), and there are data to indicate a role for cAMP in ion and water transport across the CP (4, 19, 20, 27, 73). In frog CP, cAMP has been proposed to increase HCO_3^- secretion and ion transport into CSF; furthermore in mice there is an apically localized inward rectifying chloride channel that is activated by cAMP and cAMP agonists (10, 55, 56). Thus, in the second ste of studies we evaluated whether altered cAMP levels observed in the CP might contribute to changes in pH_i and ion transport activities that could explain an increase in CSF production and hydrocephalus in the *Tg737*^{orpk} mutants.

To better compare acid-base transport mechanisms in mutant and wild-type CP and their responses to cAMP, we utilized an imaging technique with paired tissue preparations where two tissues loaded with BCECF were assayed simultaneously, minimizing variance between experiments. First, steady-state pH_i was measured in both mutant and wild-type tissues either in the absence or presence of CO_2/HCO_3^-. CP from *Tg737^{orpk}* compared to wild-type mice had a lower pH_i in both buffer conditions. We hypothesized that this was due to altered activity of either acid loading or extruding transporters. Current data indicate that CP possess a Na^+/H^+ antiporter (NHE1), Na^+-dependent HCO_3^- transporters, and a Cl^-/HCO_3^- exchanger (AE2) whose activity could contribute to the altered pH_i regulation (10). Thus, a potential caveat that must be noted in these studies is that we do not know whether there is a different profile of transporters expressed in mice at the ages used to evaluate CP epithelial transport properties in the Tg737^{orpk} mice.

To begin evaluating the cause of the difference in pH_i, we first analyzed the activity of Na^+-H^+ exchanger in mutant and wild-type tissues. However, based on our data, we could not detect a Na^+-dependent pH_i recovery following CPacidification in the nominal absence of CO_2/HCO_3^-. This would be expected if an active NHE were present on the plasma membrane. Thus, it is unlikely that this transport would contribute remarkably to the observed differences between pH_i in CP obtained from wild-type and mutant animals. Also, published data regarding the presence or activity of NHE in CP are controversial. In two studies, a basolateral amiloride-sensitive NHE was suggested to participate in Na^+ uptake into CP, assuring basolateral Na^+ supply in response to apical Na^+ flux into the CSF (15, 41). However, other groups found no evidence for the expression of a Na^+-H^+ antiporter in choroid plexus suggesting that this antiporter may not be present or that another variant may exist (1, 49).

To further investigate the mechanism behind the pH_i differences, we compared Na^+/HCO_3^- cotransporter activity in CP epithelia from mutant and wild-type animals. There are three Na^+/HCO_3^- cotransporters on CP. Two are localized to the basolateral membrane (NBCn1 and NCBE) while the other is present on the apical membrane (NBCe2) (8, 48). They all have important roles in regulating pH_i. In addition to pH_i regulation, the apically localized NBCe2 is thought to contribute directly to CSF production (49). In our studies, we found a marked increase in pH_i and calculated

HCO_3^- flux was present in both mutant and wild-type samples following Na^+ addition to acidified CP tissues. In addition, the Na^+-dependent HCO_3^- flux was significantly higher in the mutant versus wild-type samples. Based on our findings the activity of Na^+/HCO_3^- cotransport of CP showed little DIDS sensitivity at low intracellular pH_i.

We also investigated whether intracellular cAMP, which is markedly elevated in *Tg737*^{orpk} mutant choroid plexus, was able to influence Na^+-dependent HCO_3^- transport. cAMP is known to stimulate HCO_3^- flux in cornea, pancreas, and colon epithelial tissues. However, little is known about cAMP-mediated HCO_3^- transport in the mammalian choroid plexus. In our studies, we found that the addition of db-cAMP to wild-type CP does result in significantly higher Na^+-dependent HCO_3^- flux in acidified CP tissues compared to untreated control samples. These data confirm that cAMP is able to regulate Na^+-dependent HCO_3^- activity in the CP and suggest that the elevated level of cAMP observed in the mutant CP may stimulate Na^+-dependent HCO_3^- transport. To further explore this possibility, we next treated mutant CP explants with H-89, which blocks cAMP mediated effects through inhibition of protein kinase A activity. The results from these experiments indicate that blocking PKA activity markedly reduced Na^+-dependent HCO_3^- transport in mutant tissue. Taken together, these data raise the possibility that aberrant cAMP/PKA mediated signaling activity is a driving force in hydrocephalus of *Tg737*^{orpk} mutants as recently suggested for cyst development in PKD, a phenotype also present in *Tg737*^{orpk} animals.

The mechanism by which the impaired ciliary function on the CP in the *Tg737*^{orpk} mutant results in excess CSF is currently unknown. However, our data suggest at least two possibilities. In the first scenario, the cAMP mediated increased Na^+-dependent HCO_3^- transport could be the driving force that leads to the excess CSF production. Increased Na^+-dependent HCO_3^- transport activity in the mutants would cause a net increase in ion transport and subsequent fluid movement into the CSF. Indeed, data from frog CP have already established a connection between cAMP and increase HCO_3^- secretion into CSF that does lead to an increase in CSF production (55, 56). However, we note that the intracellular pH is low in our experimental conditions, well beyond the physiological range, consequently, the direction of the Na^+-dependent HCO_3^- transport is inward in acidified CP cells. *In vivo*, this is likely different, since at the estimated reversal potential of ~ -50 mV the transporter could be driven in either

direction, depending on ion/Vm conditions (38, 50). The lower pH_i of the mutant CP could be due to an increased acid loading by the apical Na^+/HCO_3^- transporter: however, based on our data, we cannot identify the localization of the Na^+/HCO_3^- transporter activated by cAMP. We also note here, that in our experimental conditions, the monitored region of interest of CP tissue is an intact epithelium, thus, epithelial responses to the change of bathing solution are probably apical events. However, since our analysis is conducted on relatively small tissue samples with cut edges, we cannot exclude accessibility of the bathing solutions to the basolateral side of the CP which could also contribute to the responses seen in our analyses.

In the second scenario we also propose a cAMP-driven effect on ion and water transport across the mutant CP. In this case, the increased ion transport would be mediated by the apically localized inward rectifying chloride channel (ClC_2 like channel). The ClC_2-like channel transports both Cl^- and HCO_3^- into the CSF and is known to be stimulated by cAMP (10, 32, 33). The first set of studies have shown that Cl^- levels in the CSF are elevated in the mutants. Thus, cAMP induced activity of this channel could explain the changes in CSF chloride levels and lower pH_i observed in the mutants with the altered Na^+-dependent HCO_3^- transport being a compensatory mechanisms responding to altered pH_i. The connection between cAMP and the activity of these transporters and channels and whether the altered activity results in increased CSF production in the *Tg737*^{orpk} mutants needs to be evaluated.

As indicated above, increased cAMP levels are a pathogenic factor leading to the development of cystic kidney disease in ARPKD and ADPKD patients and animal models (71). In the renal cystic epithelia, adenylyl cyclase activity was elevated through the vasopressin V2 receptor (V2R) (72). Furthermore, progression of the cystic pathology can be greatly retarded by the use of V2R antagonists. While V2R is not thought to be expressed in adult CP, the mRNA was reported in the CP of newborn rodents (31). Thus, it would be interesting to determine whether V2R expression is maintained in mutant CP, and whether hydrocephalus pathology can be ameliorated through administration of V2R antagonists.

CONCLUSION

The brain pathology in the *Tg737*^{orpk} mutants appears to be a consequence of several cilia dysfunction mediated events. The first, and what we believe is an initiating factor, involves altered ion transport across the CP epithelium and increased production of CSF. How impaired cilia or polaris function in the CP epithelium affect the localization, expression, or activity of proteins involved in ion movement and which proteins are specifically involved is being evaluated. One possibility is that loss of normal polaris function in the mutants results in altered distribution of a transporter/channel/exchanger in the cilia axoneme and subsequently leads to their aberrant function. The precedent for this is established in the case of polycystin-1. Polycystin-1 is required for flow induced calcium signaling mediated by deflection of the primary cilium on renal epithelium and recently, it has been shown that this flow induced calcium signal is similarly abrogated in perfused tubules from *Tg737*^{orpk} mutants (37).

Our expectation is that the loss or deformed cilia on cells of the CP may alter the function of proteins involved in ion transport and CSF production similar to what is occurring in renal epithelia of cystic kidney diseases. It is interesting to speculate that similar defects might be occurring in the epithelia of other tissues (i.e. biliary duct and pancreatic duct) affected in the *Tg737*^{orpk} mutants. Thus, understanding how cilia organize directional ion transport and CSF production in CP may provide important insights into the pathogenesis of several other diseases involving cilia dysfunction.

The second event is likely the loss of cilia beat on the ependymal cells lining the ducts and ventricles. Previous studies in mice, such as the *Mdnah5* mutant, indicate that motile cilia do have important roles in CSF movement and that loss of these motile cilia lead to hydrocephalus. Based on our analysis of when and where motile cilia form in relation to the disease pathogenesis in the *Tg737*^{orpk} mutants, it is likely that progression of the disease is exacerbated by impaired CSF movement through the ducts connecting the ventricles. This would result in increased intracranial pressure, ventricular expansion and duct stenosis with rapid progression of the disease.

Finally, our physiologic studies show that loss of normal function of the ciliogenic protein polaris in *Tg737*^{orpk} mutant mice results in a lower steady state pH_i and higher Na^+ -dependent HCO_3^- transport activity in CP. These changes are associated

with elevated levels of intracellular cAMP in the mutant tissue. Indeed, addition of a cAMP analogue was able to increase Na^+-dependent HCO_3^- transport in wild-type CP, while H-89 an inhibitor of cAMP mediated PKA activity was able to reduce HCO_3^- flux in mutant tissue. We would like to evaluate in the future whether the alteration in cAMP-mediated effects on Na^+/HCO_3^- transport activity is associated with increased CSF production that could lead to development of hydrocephalus in these mice.

BIBLIOGRAPHY

1. Alper SL, Stuart-Tilley A, Simmons CF, Brown D, Drenckhahn D. (1994) The fodrin-ankyrin cytoskeleton of choroid plexus preferentially colocalizes with apical Na+K(+)-ATPase rather than with basolateral anion exchanger AE2. J Clin Invest, 93: 1430-1438.

2. AMES A, III, SAKANOUE M, Endo S. (1964) NA, K, CA, MG, AND C1 CONCENTRATIONS IN CHOROID PLEXUS FLUID AND CISTERNAL FLUID COMPARED WITH PLASMA ULTRAFILTRATE. J Neurophysiol, 27: 672-681.

3. Avner ED. (1993) Epithelial polarity and differentiation in polycystic kidney disease. J Cell Sci Suppl, 17: 217-222.

4. Bachmann O, Rossmann H, Berger UV, Colledge WH, Ratcliff R et al. (2003) cAMP-mediated regulation of murine intestinal/pancreatic Na+/. Am J Physiol Gastrointest Liver Physiol, 284: G37-G45.

5. Bevensee MO, Weed RA, Boron WF. (1997) Intracellular pH regulation in cultured astrocytes from rat hippocampus. I. Role Of HCO3-. J Gen Physiol, 110: 453-465.

6. Bianchini L, Poussegur J. (1994) Molecular structure and regulation of vertebrate Na+/H+ exchangers. J Exp Biol, 196: 337-345.

7. Boron WF, De WP. (1976) Intracellular pH transients in squid giant axons caused by CO2, NH3, and metabolic inhibitors. J Gen Physiol, 67: 91-112.

8. Bouzinova EV, Praetorius J, Virkki LV, Nielsen S, Boron WF, Aalkjaer C. (2005) Na+-dependent. Am J Physiol Cell Physiol, 289: C1448-C1456.

9. Brown NE, Murcia NS. (2003) Delayed cystogenesis and increased ciliogenesis associated with the re-expression of polaris in Tg737 mutant mice. Kidney Int, 63: 1220-1229.

10. Brown PD, Davies SL, Speake T, Millar ID. (2004) Molecular mechanisms of cerebrospinal fluid production. Neuroscience, 129: 957-970.

11. Bruni JE, Del Bigio MR, Clattenburg RE. (1985) Ependyma: normal and pathological. A review of the literature. Brain Res, 356: 1-19.

12. Bush A. (2000) Primary ciliary dyskinesia. Acta Otorhinolaryngol Belg, 54: 317-324.

13. Cano DA, Murcia NS, Pazour GJ, Hebrok M. (2004) Orpk mouse model of polycystic kidney disease reveals essential role of primary cilia in pancreatic tissue organization. Development, 131: 3457-3467.

14. Chen J, Knowles HJ, Hebert JL, Hackett BP. (1998) Mutation of the mouse hepatocyte nuclear factor/forkhead homologue 4 gene results in an absence of cilia and random left-right asymmetry. J Clin Invest, 102: 1077-1082.

15. Davson H, Segal MB. (1970) The effects of some inhibitors and accelerators of sodium transport on the turnover of 22Na in the cerebrospinal fluid and the brain. J Physiol, 209: 131-153.

16. Davy BE, Robinson ML. (2003) Congenital hydrocephalus in hy3 mice is caused by a frameshift mutation in Hydin, a large novel gene. Hum Mol Genet, 12: 1163-1170.

17. DeMattos RB, Bales KR, Parsadanian M, O'Dell MA, Foss EM et al. (2002) Plaque-associated disruption of CSF and plasma amyloid-beta (Abeta) equilibrium in a mouse model of Alzheimer's disease. J Neurochem, 81: 229-236.

18. Doolin PF, Birge WJ. (1966) Ultrastructural organization of cilia and basal bodies of the epithelium of the choroid plexus in the chick embryo. J Cell Biol, 29: 333-345.

19. Dunk CR, Brown CD, Turnberg LA. (1989) Stimulation of Cl/HCO3 exchange in rat duodenal brush border membrane vesicles by cAMP. Pflugers Arch, 414: 701-705.

20. Emmons C, Stokes JB. (1994) Cellular actions of cAMP on HCO3(-)-secreting cells of rabbit CCD: dependence on in vivo acid-base status. Am J Physiol, 266: F528-F535.

21. Garton HJ, Piatt JH, Jr. (2004) Hydrocephalus. Pediatr Clin North Am, 51: 305-325.

22. Guay-Woodford LM. (2003) Murine models of polycystic kidney disease: molecular and therapeutic insights. Am J Physiol Renal Physiol, 285: F1034-F1049.

23. Hayashi H, Szaszi K, Grinstein S. (2002) Multiple modes of regulation of Na+/H+ exchangers. Ann N Y Acad Sci, 976: 248-258.

24. Hayashi M. (2001) Phosphorylation of a new member of the bicarbonate cotransporter superfamily. Kidney Int, 60: 462-465.

25. Hayashi M, Yamaji Y, Iyori M, Kitajima W, Saruta T. (1991) Effect of isoproterenol on intracellular pH of the intercalated cells in the rabbit cortical collecting ducts. J Clin Invest, 87: 1153-1157.

26. Haycraft CJ, Swoboda P, Taulman PD, Thomas JH, Yoder BK. (2001) The C. elegans homolog of the murine cystic kidney disease gene Tg737 functions in a ciliogenic pathway and is disrupted in osm-5 mutant worms. Development, 128: 1493-1505.

27. Hogan DL, Crombie DL, Isenberg JI, Svendsen P, Schaffalitzky de Muckadell OB, Ainsworth MA. (1997) CFTR mediates cAMP- and Ca2+-activated duodenal epithelial. Am J Physiol, 272: G872-G878.

28. Ibanez-Tallon I, Pagenstecher A, Fliegauf M, Olbrich H, Kispert A et al. (2004) Dysfunction of axonemal dynein heavy chain Mdnah5 inhibits ependymal flow and reveals a novel mechanism for hydrocephalus formation. Hum Mol Genet, 13: 2133-2141.

29. Ibraghimov-Beskrovnaya O, Dackowski WR, Foggensteiner L, Coleman N, Thiru S et al. (1997) Polycystin: in vitro synthesis, in vivo tissue expression, and subcellular localization identifies a large membrane-associated protein. Proc Natl Acad Sci U S A, 94: 6397-6402.

30. Jones HC, Bucknall RM. (1988) Inherited prenatal hydrocephalus in the H-Tx rat: a morphological study. Neuropathol Appl Neurobiol, 14: 263-274.

31. Kato Y, Igarashi N, Hirasawa A, Tsujimoto G, Kobayashi M. (1995) Distribution and developmental changes in vasopressin V2 receptor mRNA in rat brain. Differentiation, 59: 163-169.

32. Kibble JD, Garner C, Colledge WH, Brown S, Kajita H et al. (1997) Whole cell Cl- conductances in mouse choroid plexus epithelial cells do not require CFTR expression. Am J Physiol, 272: C1899-C1907.

33. Kibble JD, Trezise AE, Brown PD. (1996) Properties of the cAMP-activated C1- current in choroid plexus epithelial cells isolated from the rat. J Physiol, 496 (Pt 1): 69-80.

34. Kiefer M, Eymann R, von TS, Muller A, Steudel WI, Booz KH. (1998) The ependyma in chronic hydrocephalus. Childs Nerv Syst, 14: 263-270.

35. Lehman JM, Michaud EJ, Schoeb TR, ydin-Son Y, Miller M, Yoder BK. (2008) The Oak Ridge Polycystic Kidney mouse: modeling ciliopathies of mice and men. Dev Dyn, 237: 1960-1971.

36. Lindeman GJ, Dagnino L, Gaubatz S, Xu Y, Bronson RT et al. (1998) A specific, nonproliferative role for E2F-5 in choroid plexus function revealed by gene targeting. Genes Dev, 12: 1092-1098.

37. Liu W, Murcia NS, Duan Y, Weinbaum S, Yoder BK et al. (2005) Mechanoregulation of intracellular Ca2+ concentration is attenuated in collecting duct of monocilium-impaired orpk mice. Am J Physiol Renal Physiol, 289: F978-F988.

38. McAlear SD aBM. pH regulation in non-neuronal brain cells and interstitial fluid. 31, 707-745. 2004. *Advances in Molecular and Cell Biology* .
Ref Type: Generic

39. Moore A, Escudier E, Roger G, Tamalet A, Pelosse B et al. (2006) RPGR is mutated in patients with a complex X linked phenotype combining primary ciliary dyskinesia and retinitis pigmentosa. J Med Genet, 43: 326-333.

40. Moyer JH, Lee-Tischler MJ, Kwon HY, Schrick JJ, Avner ED et al. (1994) Candidate gene associated with a mutation causing recessive polycystic kidney disease in mice. Science, 264: 1329-1333.

41. Murphy VA, Johanson CE. (1989) Alteration of sodium transport by the choroid plexus with amiloride. Biochim Biophys Acta, 979: 187-192.

42. Nauli SM, Alenghat FJ, Luo Y, Williams E, Vassilev P et al. (2003) Polycystins 1 and 2 mediate mechanosensation in the primary cilium of kidney cells. Nat Genet, 33: 129-137.

43. Pazour GJ, Baker SA, Deane JA, Cole DG, Dickert BL et al. (2002) The intraflagellar transport protein, IFT88, is essential for vertebrate photoreceptor assembly and maintenance. J Cell Biol, 157: 103-113.

44. Pazour GJ, Dickert BL, Vucica Y, Seeley ES, Rosenbaum JL et al. (2000) Chlamydomonas IFT88 and its mouse homologue, polycystic kidney disease gene tg737, are required for assembly of cilia and flagella. J Cell Biol, 151: 709-718.

45. Plotkin MD, Kaplan MR, Peterson LN, Gullans SR, Hebert SC, Delpire E. (1997) Expression of the Na(+)-K(+)-2Cl- cotransporter BSC2 in the nervous system. Am J Physiol, 272: C173-C183.

46. Praetorius HA, Spring KR. (2003) The renal cell primary cilium functions as a flow sensor. Curr Opin Nephrol Hypertens, 12: 517-520.

47. Praetorius HA, Spring KR. (2005) A physiological view of the primary cilium. Annu Rev Physiol, 67: 515-529.

48. Praetorius J. (2007) Water and solute secretion by the choroid plexus. Pflugers Arch, 454: 1-18.

49. Praetorius J, Nielsen S. (2006) Distribution of sodium transporters and aquaporin-1 in the human choroid plexus. Am J Physiol Cell Physiol, 291: C59-C67.

50. Pushkin A, Kurtz I. (2006) SLC4 base (HCO3 -, CO3 2-) transporters: classification, function, structure, genetic diseases, and knockout models. Am J Physiol Renal Physiol, 290: F580-F599.

51. Putney LK, Denker SP, Barber DL. (2002) The changing face of the Na+/H+ exchanger, NHE1: structure, regulation, and cellular actions. Annu Rev Pharmacol Toxicol, 42: 527-552.

52. Rolf B, Kutsche M, Bartsch U. (2001) Severe hydrocephalus in L1-deficient mice. Brain Res, 891: 247-252.

53. Romero MF, Fulton CM, Boron WF. (2004) The SLC4 family of HCO 3 - transporters. Pflugers Arch, 447: 495-509.

54. Rosenbaum JL, Witman GB. (2002) Intraflagellar transport. Nat Rev Mol Cell Biol, 3: 813-825.

55. Saito Y, Wright EM. (1983) Bicarbonate transport across the frog choroid plexus and its control by cyclic nucleotides. J Physiol, 336: 635-648.

56. Saito Y, Wright EM. (1984) Regulation of bicarbonate transport across the brush border membrane of the bull-frog choroid plexus. J Physiol, 350: 327-342.

57. Sapiro R, Kostetskii I, Olds-Clarke P, Gerton GL, Radice GL, Strauss III JF. (2002) Male infertility, impaired sperm motility, and hydrocephalus in mice deficient in sperm-associated antigen 6. Mol Cell Biol, 22: 6298-6305.

58. Scholey JM. (2003) Intraflagellar transport. Annu Rev Cell Dev Biol, 19: 423-443.

59. Schuster VL. (1986) Cyclic adenosine monophosphate-stimulated anion transport in rabbit cortical collecting duct. Kinetics, stoichiometry, and conductive pathways. J Clin Invest, 78: 1621-1630.

60. Segal MB. (2001) Transport of nutrients across the choroid plexus. Microsc Res Tech, 52: 38-48.

61. Strazielle N, Ghersi-Egea JF. (2000) Choroid plexus in the central nervous system: biology and physiopathology. J Neuropathol Exp Neurol, 59: 561-574.

62. Sullivan LP, Wallace DP, Grantham JJ. (1998) Epithelial transport in polycystic kidney disease. Physiol Rev, 78: 1165-1191.

63. Supp DM, Brueckner M, Kuehn MR, Witte DP, Lowe LA et al. (1999) Targeted deletion of the ATP binding domain of left-right dynein confirms its role in specifying development of left-right asymmetries. Development, 126: 5495-5504.

64. Sutters M, Germino GG. (2003) Autosomal dominant polycystic kidney disease: molecular genetics and pathophysiology. J Lab Clin Med, 141: 91-101.

65. Takeda S, Yonekawa Y, Tanaka Y, Okada Y, Nonaka S, Hirokawa N. (1999) Left-right asymmetry and kinesin superfamily protein KIF3A: new insights in determination of laterality and mesoderm induction by kif3A-/- mice analysis. J Cell Biol, 145: 825-836.

66. Taulman PD, Haycraft CJ, Balkovetz DF, Yoder BK. (2001) Polaris, a protein involved in left-right axis patterning, localizes to basal bodies and cilia. Mol Biol Cell, 12: 589-599.

67. Taylor J, Hamilton KL, Butt AG. (2001) Pflugers Arch, 442: 256-262.

68. Thomas JA, Buchsbaum RN, Zimniak A, Racker E. (1979) Intracellular pH measurements in Ehrlich ascites tumor cells utilizing spectroscopic probes generated in situ. Biochemistry, 18: 2210-2218.

69. Torikata C, Kijimoto C, Koto M. (1991) Ultrastructure of respiratory cilia of WIC-Hyd male rats. An animal model for human immotile cilia syndrome. Am J Pathol, 138: 341-347.

70. Torres VE. (2004) Cyclic AMP, at the hub of the cystic cycle. Kidney Int, 66: 1283-1285.

71. Torres VE. (2004) Therapies to slow polycystic kidney disease. Nephron Exp Nephrol, 98: e1-e7.

72. Wang X, Gattone V, Harris PC, Torres VE. (2005) Effectiveness of vasopressin V2 receptor antagonists OPC-31260 and OPC-41061 on polycystic kidney disease development in the PCK rat. J Am Soc Nephrol, 16: 846-851.

73. Wigham CG, Turner HC, Swan J, Hodson SA. (2000) Modulation of corneal endothelial hydration control mechanisms by Rolipram. Pflugers Arch, 440: 866-870.

74. Wilson PD. (1997) Epithelial cell polarity and disease. Am J Physiol, 272: F434-F442.

75. Yoder BK, Richards WG, Sommardahl C, Sweeney WE, Michaud EJ et al. (1996) Functional correction of renal defects in a mouse model for ARPKD through expression of the cloned wild-type Tg737 cDNA. Kidney Int, 50: 1240-1248.

76. Yoder BK, Richards WG, Sommardahl C, Sweeney WE, Michaud EJ et al. (1997) Differential rescue of the renal and hepatic disease in an autosomal recessive polycystic kidney disease mouse mutant. A new model to study the liver lesion. Am J Pathol, 150: 2231-2241.

77. Yoder BK, Tousson A, Millican L, Wu JH, Bugg CE, Jr. et al. (2002) Polaris, a protein disrupted in orpk mutant mice, is required for assembly of renal cilium. Am J Physiol Renal Physiol, 282: F541-F552.

78. Zhang Q, Davenport JR, Croyle MJ, Haycraft CJ, Yoder BK. (2005) Disruption of IFT results in both exocrine and endocrine abnormalities in the pancreas of Tg737(orpk) mutant mice. Lab Invest, 85: 45-64.

79. Zhang Q, Murcia NS, Chittenden LR, Richards WG, Michaud EJ et al. (2003) Loss of the Tg737 protein results in skeletal patterning defects. Dev Dyn, 227: 78-90.

BIBLIOGRAPHY OF THE CANDIDATE

List of publication related to the thesis

Banizs B, Komlosi P, Bevensee MO, Schwiebert EM, Bell PD, Yoder BK. Altered intracellular pH regulation and Na+ transporter activity in choroid plexus of the cilia defective Tg737orpk mutant mouse. *Am J Physiol Cell Physiol*. 2007 Apr;292(4):C1409-16. PMID: 17182727

Banizs B, Pike MM, Millican LA, Ferguson WA, Komlosi P, Sheetz J, Bell PD, Schwiebert EM, Yoder BK. Cilia malformation leads to altered ependyma and choroid plexus function and to the formation of hydrocephalus. *Development.* 2005 Dec;132(23):5329-39.

Haycraft CJ, **Banizs B**, Aydin-Son Y, Zhang Q, Michaud ED, Yoder BK. Gli2 and Gli3 Localize to Cilia and Require the Intraflagellar Transport Protein Polaris for Processing and Function. *PLoS Genetics.* 2005 Oct;1(4):e53. Epub 2005 Oct 28.

Other publications

Komlosi P, **Banizs B**, Fintha A, Steele S, Zhang ZR, Bell PD. Oscillating cortical thick ascending limb cells at the juxtaglomerular apparatus. J Am Soc Nephrol. 2008 Oct;19(10):1940-6. Epub 2008 Jun 18. PubMed PMID: 18562570; PubMed Central PMCID: PMC2551563.

Jones C, Roper VC, Foucher I, Qian D, **Banizs B**, Petit C, Yoder BK, Chen P. Ciliary proteins link basal body polarization to planar cell polarity regulation. *Nat Genet*. 2007 Dec 9; PMID: 18066062

Nakayama M, Both GW, **Banizs B**, Tsuruta Y, Yamamoto S, Kawakami Y, Douglas JT, Tani K, Curiel DT, Glasgow JN. An adenovirus serotype 5 vector with fibers derived from ovine atadenovirus demonstrates CAR-independent tropism and unique biodistribution in mice. *Virology*. 2006 Jun 20;350(1):103-15. Epub 2006 Mar 3.

Csukas Z, **Banizs B**, Rozgonyi F. Studies on the cytotoxic effects of Propionibacterium acnes strains isolated from cornea. *Microb Pathog*. 2004 Mar;36(3):171-4.

Jeney Cs, **Banizs B**, Dobay O, Glatz K, Huszar T, Adam E, Nasz I: The endosomal epsilon-cop protein is involved in human adenovirus type 5 internalization. *Acta Vet. Hung*. 2002;50(4):481-9.

ACKNOLEDGEMENT

I would like to thank from the bottom of heart:

Dr. Bradley K. Yoder Professor, Division of Cell Biology, at the University of Alabama at Birmingham, my mentor, who helped and supported my research work with great enthusiasm.

Dr. P. Darwin Bell, Professor and Head of the Renal Biology Laboratory at the Medical University of South Carolina, who contributed greatly to my research work through professional discussions and by giving me the possibility to run the physiological experiments in his lab.

I would like to thank **Dr. László Rosivall**, Professor of Pathophysiology, Nephrology Research and Training Center, Institute of Pathophysiology, Faculty of Medicine, Semmelweis University, Budapest, Ph.D. Program Director, for supporting and mentoring my Ph.D. work.

I am grateful to **Dr. Courtney J. Haycraft,** Assistant Professor in the Renal Biology Laboratory at the Medical University of South Carolina, who reviewed my papers and gave my many great professional advices.

I would like to thank **Dr. Peter Komlosi** for the professional discussions related to my research.

I also would like to thank my colleagues at the University of Alabama at Birmingham for their support and friendly atmosphere.

I cordially dedicate my work to Dr. Peter Komlosi and my parents Eva Varga and Dr. Karoly Banizs, my children, Gergely and Daniel.

ABSTRACT

Hydrocephalus is a progressive pathological condition characterized by excessive accumulation of cerebrospinal fluid (CSF) in the brain ventricles. The treatment strategies for this condition are fairly limited; a better understanding of the underlying pathomechanism is expected to provide novel therapeutic avenues. Cilia are complex organelles involved in sensory perception and fluid/cell movement. They are constructed through a highly conserved process called intraflagellar transport (IFT). Mutations in IFT genes, such as *Tg737*, result in severe developmental defects and disease including cystic kidney disease, and hydrocephalus. While cilia on the ependymal cells are motile and loss of motility has been associated with hydrocephalus, the function of cilia on the choroid plexus remains enigmatic. Our hypothesis is that cilia function is required for normal regulation of pathways governing CSF production and homeostasis. Here, we explore the connection between cilia dysfunction and the development of hydrocephalus by using the *Tg737*^{orpk} mutants. Our analysis indicates that cilia on ependyma of *Tg737*^{orpk} mutant mice are severely malformed. These defects lead to disorganized beating and impaired CSF movement. However, the loss of the cilia beat and CSF flow is not the initiating factor, as the pathology is present prior to the development of motile cilia on these cells and CSF flow is not impaired at early stages of the disease. Rather, our results suggest that loss of cilia leads to altered function of the choroid plexus epithelium, as evidenced by elevated intracellular cAMP levels and increased chloride concentration in the CSF. To evaluate hydrocephalus association with defects in ion transport in *Tg737*^{orpk} mice, we compared the steady-state pH_i and Na^+-dependent transport activities of isolated CP tissues from *Tg737*^{orpk} mutant and wild-type mice. The data indicate that *Tg737*^{orpk} mutant CP epithelium have lower pH_i and higher Na^+-dependent HCO_3^- transport activity. In addition, wild-type choroid plexus epithelium could be converted to a mutant phenotype with regard to the activity of Na^+-dependent HCO_3^- transport by addition of dibutyryl-cAMP and mutant choroid plexus epithelium toward the wild-type phenotype by inhibiting PKA activity with H-89. Together, these data suggest that cilia function is necessary for regulating ion transport and CSF production, as well as for CSF flow through the ventricles and that ciliary dysfunction in *Tg737*^{orpk} mutants disrupts a signaling pathway leading to elevated intracellular cAMP levels and aberrant regulation of pH_i and ion transport activity.

ABSZTRAKT

A hidrokefalusz progresszív patológiai folyamat, melynek jellemzője a kóros folyadékgyülem az agykamra rendszeren belül. Gyógyításában reméljük, hogy a patomechanizmus mélyebb megismerésével hatékonyabb gyógyászati eszközökkel fogunk rendelkezni. A cíliumok összetett képletek, melyek többek között szerepet játszanak az érzékelésben, sejtmozgásban és anyagok/folyadék mozgatásában. A cílium ősi struktura, melynek intraflagelláris transzportja (IFT) változatlan formaban maradt fenn az evolúció során. Az IFT fehérjék mutációja, így a *Tg737* gén károsodása is, súlyos fejlődési rendellenességeket eredményez, mint a policisztás vesebetegség és a hidrokefalusz kialakulása *Tg737*^{orpk} egerekben. Jelen célunk kideríteni, hogy a *Tg737* gén mutációja az ependíma, valamint a choroid plexus (CP) cíliumokon miként okoz kóros folyadékgyülemet az agykamrákon belül a mutáns egerekben. Kutatási eredményeink arra utalnak, hogy a cíliumok a mutáns ependímán mind morfológiailag, mind funkcionálisan súlyosan károsodottak, de megfigyeltük, hogy a kóros folyadékgyülem és a kitágult kamrák már jelen vannak a motilis cílium megjelenése előtt, továbbá hogy az aqueduktusz is átjárható a betegség kezdeti stádiumában, ami arra utal, hogy más faktor(ok) indithatják a kórfolyamatot. Következő lépésként megvizsgáltuk mutáns és egészséges egerek CP-nak cAMP szintjét, mivel ez az intracelluláris molekula bizonyítottan szerepet játszik több transzport hámsejt ion–szekréciójának szabályozásában, így a CP klór csatornájának működésében is. Kimutattuk, hogy a CP intracelluláris cAMP szintje valamint a CSF klorid ion koncentrációja magasabb volt a mutáns állatokban. A továbbiakban megvizsgáltuk a CP-ok intracelluláris pH-ját, mely alacsonyabb, és a nátrium–dependens bikarbonát transzport aktivitását, ami emelkedett volt a mutáns állatokban. Érdekes módon a vad típusú CP bicarbonát transzportere „mutáns" viselkedésűvé volt alakítható db-cAMP hozzáadásával, míg megfordítva, H-89 protein kináz A blokkoló használatával a mutáns szövet „vad típusúvá" volt alakítható. Ezek az eredmények arra utalnak, hogy a mutáns állatok CP-ában súlyos ion transzport zavarok állnak fenn. Összefoglalva, úgy gondoljuk, hogy a hidrokefalusz a *Tg737*^{orpk} mutáns egerekben a cíliumok több szinten jelentkező működési zavarának az eredménye. A CP deformált cíliumai zavart okoznak az ion transzportban résztvevő fehérjék működésében valószínűleg a megváltozott intracelluláris jelátviteli láncolaton keresztül.